Experimental techniques for hydro-mechanical and electro-chemo-hydraulic processes

Enrique Romero*-Guido Musso-Cristina Jommi*****

** Universitat Politècnica de Catalunya*
Department of Geotechnical Engineering and Geosciences
c/ Jordi Girona, 1-3, Campus Nord UPC, Building D-2
08034 Barcelona - Spain
enrique.romero-morales@upc.edu

***Politecnico di Torino*
Dipartimento di Ingegneria Strutturale, Edile e Geotecnica
Corso Duca degli Abruzzi, 24
10129 Torino, Italy

****Politecnico di Milano*
Dipartimento di Ingegneria Strutturale
piazza Leonardo da Vinci, 32
20133 Milano, Italy

This chapter presents the fundamentals behind selected experimental techniques used to control and monitor some coupled multi-physics processes. The starting point is the review of the experimental techniques for coupled hydro-mechanical testing (liquid and vapour transfer techniques). Then, fundamentals of physical processes related to electrical techniques for the characterisation of geomaterials and for the induction of coupled electro-chemo-hydraulic processes are provided. Complementary aspects concerning the application of these techniques and some of their limitations are also discussed. Selected data from tests on a clayey silt in an electrokinetic oedometer are finally shown, to provide evidence of some effects of the coupled electro-chemo-hydraulic response of soils.

1 Introduction

The extension of geotechnical engineering applications and the research interest in multi-physics processes are becoming wider in recent years, mainly within the context of geoenvironmental, energy production, and geosciences areas. Topics such as crystal growth in geomechanics, natural risk analyses (fast sliding processes along faults and landslide surfaces), biological soil improvement, geothermal energy exploitation, waste confinement (at surface or at great depths using engineered barriers or host geological formations), soil pollution and remediation, carbon dioxide sequestration in geological formations, oil field subsidence phenomena and assessment of seals in hydrocarbon production, to cite but a few of them, are increasingly coming into prominence. These new fields of application require the incorporation of relevant and coupled thermo-hydro-chemo-bio-electro-mechanical phenomena, the evolution of which must be examined over important periods of time, and the introduction of new constitutive variables for a deeper understanding of the behaviour of geomaterials. Progress in these areas requires advanced experimental techniques, fundamental developments and numerical modelling, as well as detailed examination of well documented field cases. Within this context, the present chapter introduces selected experimental techniques to investigate hydro-mechanical and electro-chemo-hydraulic processes. The fundamental bases are first introduced, followed by descriptions on how these techniques are implemented. Complementary aspects concerning some of their limitations are also presented.

2 Hydro-mechanical processes

2.1 Introduction

This section focuses on the description of two widely used techniques to transfer and control the amount of water inside a porous medium; namely

- Axis translation technique that predominantly transfers (and controls) liquid phase through an interface permeable to dissolved salts, and that is related to the control of matric suction (i.e., difference between the gas and liquid phases); and
- Vapour equilibrium technique to transfer vapour through the gas phase, which is associated with the control of the relative humidity or total suction.

2.2 Axis translation technique for controlling liquid transfer

Axis translation is one of the most commonly used techniques for controlling matric suction, together with osmotic technique. The reader interested in osmotic technique is referred to [Del08a, Del08b, Tan11 and Bla08]. The pressure plate outflow technique is an early example of the use of axis translation technique [Ric41, Gar56].

This technique is associated with the matric suction component, in which water potential is controlled by liquid phase transfer through a saturated interface –usually saturated high air-entry value (HAEV) ceramic disk or saturated symmetric cellulose acetate membrane– that is permeable to dissolved salts. The procedure involves the translation of the reference pore air pressure, through an artificial increase of the atmospheric pressure Δu_a in which the soil is immersed. The procedure is described in Figure 1 for a setup corresponding to an isotropic cell with HAEV ceramic disk at the bottom and coarse porous disk at the top. Consequently, the negative pore water pressure increases by an equal amount if incompressibility of soil particles and water is assumed –i.e., if the curvature of the menisci is not greatly affected–. This translation of the pore water pressure into the positive range allows its measurement [Hil56], and consequently, its control if water pressure is regulated through a saturated interface in contact with the sample. To cover a wide matric suction range, the soil should preferably present a lower air-entry value than the corresponding one of the ceramic disk. To ensure that the top boundary presents no water flow condition, the top coarse porous disk should display a very low air-entry value (this ensures that no water is stored when applying matric suction), as indicated in Figure 1. Alternative combinations of porous disks can be used in a single cap; for example by surrounding the ceramic disk by a coarse porous ring through which air pressure is applied. Axis translation technique has been experimentally evaluated with soils having a continuous air phase and a degree of saturation varying between 0.76 and 0.95 by [Fre77] and by [Tar00] for degrees of saturation between 0.56 and 0.77. Further details of the physical fundamentals and implementation of the technique can be found in [Del08a, Hoy08, Mar08, Mas08 and Van08].

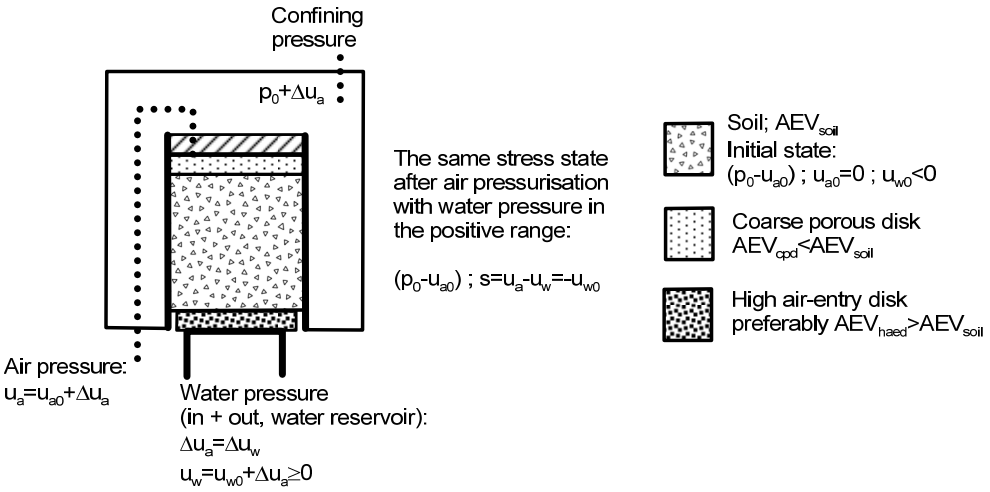

Figure 1: Axis translation application in an isotropic cell with bottom HAEV ceramic disk and top coarse porous disk.

Axis translation technique has been criticised concerning the following aspects: a) it

is not representative of field conditions, where air pressure is usually under atmospheric conditions (some authors have argued that axis translation alters soil behaviour by preventing cavitation; see for instance [Bak09]); b) there are some doubts in how the air pressurisation process affects the water pressure when water is held by adsorption mechanisms; and, finally c) it is not clear its application at nearly saturated states in the absence of a continuous gaseous phase. Nevertheless, axis translation technique has proved to provide reasonable results and a good continuity between vapour equilibrium results at elevated suctions and nearly saturated states. An example can be found in Figure 2, in which the overall picture of water retention results under constant volume conditions of an artificially prepared expansive clay (with pellets of Febex bentonite) were obtained by combining different techniques (transistor psychrometers and vapour control technique) jointly with axis translation [Hof05]. A recent benchmark aimed at comparing different experimental techniques for controlling/measuring suction (axis translation, osmotic technique, high-capacity tensiometer and dew-point psychrometer) on a mixture of kaolinite, bentonite and sand (reference soil), was presented by [Tar11]. The same techniques were tested by different laboratories and similar results were obtained for the water retention curves of the reference soil, which gives further confidence on the use of this technique.

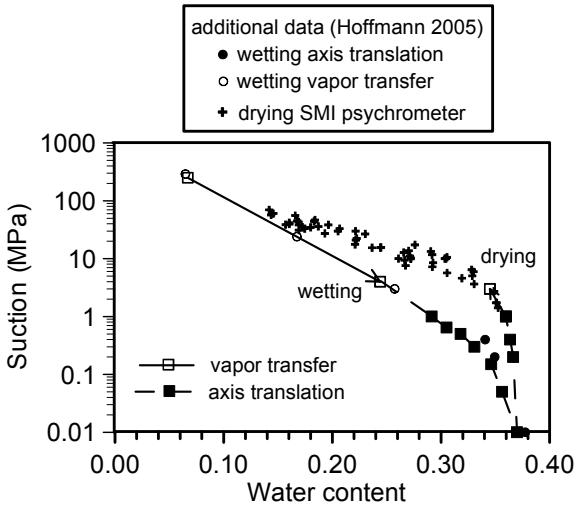

Figure 2: Water retention curves obtained by combining axis translation with other techniques [Hof05].

Main experimental difficulties concerning axis translation application are associated with the accumulation of diffused air beneath the HAEV ceramic disk, the control of the relative humidity of the air chamber to minimise evaporation or condensation effects on the sample, the application of the air pressurisation process at elevated degrees of saturation, and the estimation of the equalisation time.

In relation to air diffusion problems through the saturated porous network of the interface, it can induce the progressive loss of continuity between the pore water and the water in the control system. In addition, the accumulation of air can lead to water volume change errors in drained tests and pore-water pressure measurement errors in undrained tests. Consequently, an auxiliary device is required to flush periodically air bubbles accumulated below the HAEV ceramic. The following expression describes the rate of accumulation of dissolved air beneath the ceramic disk, which is based on the gradient of air concentration being the driving mechanism [Fre93, Rom99]:

$$\frac{dV_d}{dt} = \frac{n\,A\,D\,h\,(u_a - u_w)}{(u_w + u_{atm})\,t_c} \tag{1}$$

where n, A and t_c, represent the porosity (usually between 0.32 and 0.38 for commercial ceramics), the cross-sectional area and the disk thickness, respectively. h, is the volumetric coefficient of solubility of dissolved air in water (h=0.018 at 22°C), and D, the diffusion coefficient through the saturated interface. u_{atm}, represents the absolute atmospheric pressure; u_a and u_w refer to air and water gauge pressures. The quantification of air diffusion has been recently carried out by [Rom01a, DeG02, Air05 and Pad06]. Lawrence et al. [Law05] presented a pressure pulse technique for measuring diffused air volume using pressure/volume controllers. Figure 3a presents values of the coefficient of diffusion of air through a saturated ceramic disk with a nominal air-entry value of 1.5 MPa as a function of applied matric suction. Typical values are in the range between 3×10^{-11} and 2×10^{-10} m^2/s (for suctions < 0.7 MPa), lower than the values of diffusion of air in water (around 2.2×10^{-9} m^2/s at 20°C). Factors such as tortuosity of the paths and breakdown of Henry's law in a curved air-water interface can be associated with this reduction [Bar67]. The figure shows how this coefficient tends to increase as suction increases over 0.7 MPa and gets closer to the air-entry value of the ceramic (the value at which the gas convection transport is initiated). Figure 3b shows the pore size density function of a HAEV ceramic (nominal air-entry value 1.5 MPa and porosity 0.324) obtained by mercury intrusion porosimetry, in which a dominant pore size mode of 81 nm is obtained. The water retention curve obtained by mercury intrusion porosimetry of the ceramic is shown in Figure 3c. An air-entry value between 1.6 and 2 MPa is detected, which is slightly larger than the nominal value. Despite this higher value, the important air diffusion rates at suctions > 1 MPa indicate that the technique has some practical limitations when commercial ceramics are used. As deduced from Equation (1), increasing the water pressure is an efficient way to reduce air diffusion rates for a given geometry of the interface element and for specified matric suction. The conventional technique of the pressure plate apparatus, in which the pressure of water is maintained under atmospheric conditions, is the less efficient configuration to control the diffusion of air.

Concerning the second phenomenon of vapour transfer between the soil and the surrounding air, it can be controlled by maintaining an adequate relative humidity in

the air chamber (around 95%). Evaporative fluxes are originated due to the difference in vapour pressure between the soil surface and the air chamber. Volumetric evaporative fluxes can be detected in the water volume change device as a non-stop inflow to the soil under steady-state conditions. Condensation of vapour in the internal walls of the pressure chamber due to temperature variations has also been reported by [Oli06].

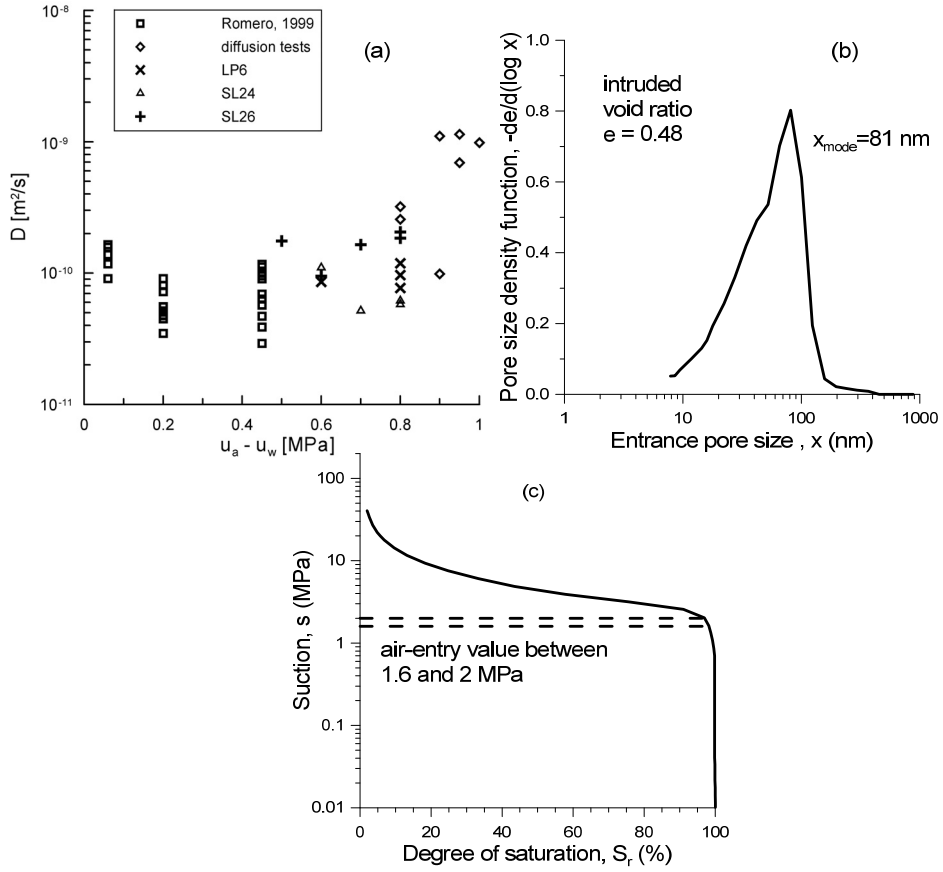

Figure 3: a) Diffusion coefficients for air through saturated ceramic disk (nominal air-entry value 1.5 MPa) for different matric suctions [Air05]. b) Pore size density function of HAEV ceramic disk (nominal air-entry value 1.5 MPa). c) Water retention curve of HAEV ceramic disk obtained by mercury intrusion porosimetry (nominal air-entry value 1.5 MPa).

Measured volumetric evaporative fluxes at different porosities are presented in Figure 4 for compacted clay inside an air chamber at an initial relative humidity h_{r0}=0.50. As shown in the scheme, two different water fluxes are involved in the process: a) an evaporative flux that dries the clay surface (dependent on soil proper-

ties –mainly vapour diffusivity– and on boundary conditions –h_r of air chamber above the evaporating surface–), and b) a liquid flux through the ceramic disk that regulates the applied matric suction and depends on soil and ceramic disk water permeability.

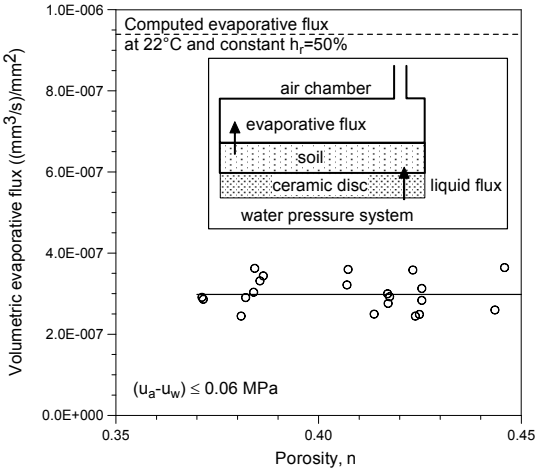

Figure 4: Measured volumetric evaporative fluxes [Rom99].

A series of 1-D numerical analyses using Code_Bright [Oli96] was carried out by [Rom99] to simulate evaporative fluxes and matric suction evolution during a wetting path performed on compacted clay. The analysis took into account liquid phase flow by Darcy's law and vapour diffusion according to Fick's law. The clay saturated permeability was 8.3×10^{-12} m/s, with the following power expression for the liquid relative permeability: $k_{rl} = S_e^{2.89}$ (the effective saturation is computed as $S_e = (S_r - 0.087)/0.913$, where S_r is the degree of saturation). S_e is computed as a function of matric suction: $S_e = [1+((u_a-u_w)/P)^{1/(1-\lambda)}]^{-\lambda}$, where $\lambda = 0.156$ and $P = 0.03$ MPa. The ceramic disk displayed a saturated permeability of 1.3×10^{-10} m/s. A tortuosity factor of 0.30 was considered, which accounts for complexities in pore geometry affecting vapour diffusion in air. Figure 5 shows the time evolution of matric suction during the wetting path for three representative points of the 10-mm sample (top in contact with coarse porous disk, mid-height and bottom in contact with ceramic disk), starting from an initial value $(u_a-u_w)_0$=1.9 MPa to $(u_a-u_w)_f$=0.45 MPa. An initial relative humidity of the air chamber h_{r0}=0.50 was assumed in accordance to the relative humidity of the laboratory. Two different systems were analysed. In the open system, a constant relative humidity of h_r=0.50 was prescribed along the wetting stage at the top surface of the sample in contact with the air chamber (refer to the scheme shown in Figure 4). On the other hand, in the closed system simulation the relative humidity progressively increased towards a final value h_r= 0.996. According to Figure 5, water evaporation will cause an initial drying on the clay upper surface. This drying progressively slows down and reverses as liquid water flows into the sample. On the contrary, a monotonic suction decrease is detected at the bottom

boundary of the sample. As observed in the figure, at the end of the wetting path, full matric suction equalisation throughout the sample height is not attained in the open system (matric suction at the top of the sample presents a value of 0.50 MPa under steady-state conditions). This is why it is important to ensure a high h_r in the air pressure system or alternatively control the volumetric evaporative flux measured under steady-state conditions. A maximum volumetric evaporative flux of 9.4×10^{-7} $(mm^3/s)/mm^2$ was computed, when h_r=0.5 was imposed in the air chamber. For measured volumetric evaporative fluxes lower than this value, no important consequences are expected and a relatively uniform matric suction distribution is expected throughout the sample height [Rom99,01a,b] (refer to Figure 4).

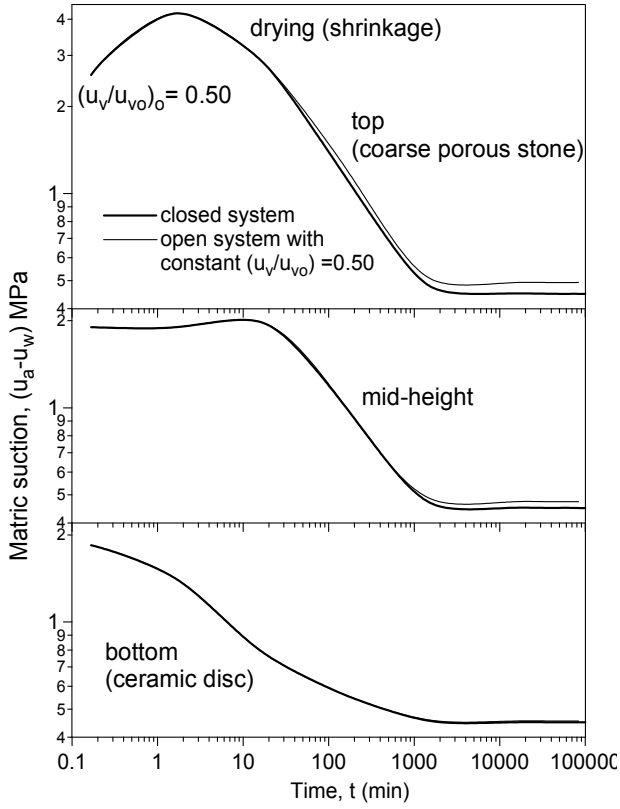

Figure 5: Numerical results of matric suction evolution at three different elevations during a wetting stage from s=1.9 MPa to 0.45 MPa [Rom99].

The application of air pressure at elevated degrees of saturation can induce irreversible arrangements in soil skeleton due to pore fluid compression (occluded air bubbles). Bocking and Fredlund [Boc80] studied the effect of occluded air during the use of axis translation technique. If nearly saturated states are expected to be reached

during the hydraulic paths, it is preferable to increase air pressure when the continuity of air is ensured (degrees of saturation < 0.85), and then maintain the continuous air phase at constant pressure. This can be observed in Figure 2, in which the drying path followed a wetting path that attained very low matric suctions (10 kPa). Throughout this hydraulic process, air pressure was maintained constant and suction was changed by manipulating water pressure.

One important difficulty when using axis translation technique is the estimation of the time required to reach suction equalisation. Water volume measurements are usually affected by the relative humidity of the air chamber and the diffusion of air. Although these phenomena can be minimised as previously suggested, the estimation of the equalisation time in oedometer and triaxial cells has been conventionally determined based on overall soil volume change measurements that are independently determined. Oliveira and Marinho [Oli06] studied the equilibration time in the pressure plate and recommended around three days for increments from 50 kPa to 100 kPa for gneissic soils. From the analytical solution proposed by [Kun62], which considers the ceramic disk impedance and the soil permeability to determine the time evolution of the water volume change in a soil with a rigid matrix, it is possible to estimate an equalisation time t_{95} for which 95% of the water outflow or inflow has occurred (for simplicity only one term of the Fourier series has been considered):

$$
\begin{aligned}
& t_{95} \approx -\frac{L^2}{\alpha_1{}^2 D} \ln\left[\frac{\alpha_1{}^2}{40}(a+\csc^2\alpha_1)\right]; \\
& a\alpha_1 = \cot\alpha_1 \quad \text{with} \quad 0 < \alpha_1 \le \frac{\pi}{2}; \\
& D = -\frac{k_w}{n\gamma_w}\frac{\delta s}{\delta S_r}
\end{aligned}
\tag{2}
$$

where L is the soil height (longest drainage path); D the capillary diffusivity that is assumed constant and is dependent on water permeability, k_w, and soil water capacity, $\delta s/\delta S_r$ (s is the matric suction, S_r the degree of saturation, n the porosity, and γ_w the unit weight of water); a the ratio of impedance of the ceramic disk to the impedance of the soil $a = k_w t_c/(Lk_d)$ (t_c is the ceramic disk thickness and k_d its water permeability), and α_1 the solution of the equation in the indicated range. For low disk impedance, $a \approx 0$ and $\alpha_1 \approx \pi/2$, the minimum equalisation time can be approximately estimated as:

$$
t_{95} \approx 1.129\frac{L^2}{D} \tag{3}
$$

For a clayey soil with L = 20 mm, $n = 0.48$, $k_w = 5\times10^{-12}$ m/s and $\delta s/\delta S_r \approx -2.8$ MPa in the suction range $0.1\,\text{MPa} < s < 0.5\,\text{MPa}$, and disk properties t_c = 7 mm and $k_d = 10^{-10}$ m/s, then $a \approx 0.018$, $\alpha_1 \approx 1.543$, $D \approx 3.0\times10^{-9}$ m^2/s and t_{95}

≈ 2615 min. It is important to remark that this estimation is based on a constant soil volume consideration, which is not exactly the case of a clayey soil. Nevertheless, it gives an approximate estimation of the minimum time required to reach suction equalisation.

2.3 Vapour transfer technique

Vapour equilibrium technique is implemented by controlling the relative humidity h_r of a closed system. Soil water potential is controlled by means of the migration of water molecules through the vapour phase from a reference system of known potential to the soil pores, until equilibrium is achieved. The thermodynamic relation between total suction ψ of soil moisture and the h_r of the reference system is given by the psychrometric law [Fre93]. The h_r of the reference system can be controlled by varying the chemical potential of different types of aqueous solutions [Lid97, Del98, Tan05]. Figure 6 shows the relationship between ψ and the concentration of NaCl aqueous solution (molality, m, mol of NaCl / kg of pure water). The upper limit is controlled by the salt solubility that restricts h_r=0.75 at 20°C.

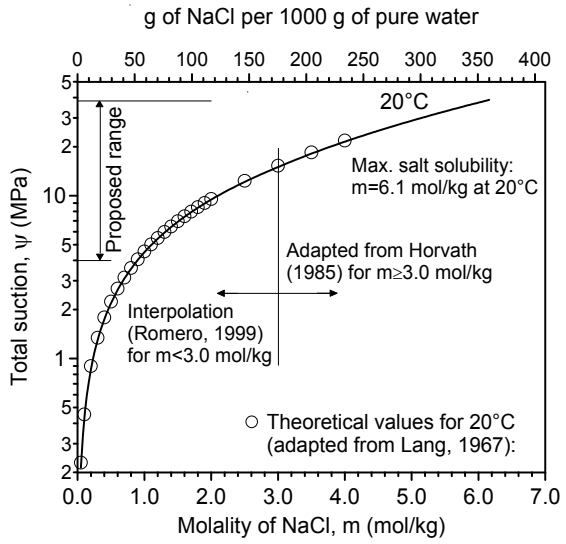

$$h_r = 1 - 0.035m - \chi m(m-3)$$

$$\chi = 1.739 \times 10^{-3} \text{ for } m \geq 3 \text{ mol/kg}$$

$$\chi = 1.142 \times 10^{-3} \text{ for } m < 3 \text{ mol/kg}$$

Figure 6: Total suction application with partially saturated NaCl solutions [Hor85, Rom99].

Oedometer cells installed inside a chamber with relative humidity control were used by [Est90, Ber97, Vil99, Cui05]. The main drawback of this experimental setup is that the time to reach moisture equalisation is extremely long due to the fact that vapour transfer depends on diffusion (several weeks are required for each suction step in the case of high-density clays as observed in Figure 7). In order to speed up

the process, vapour transfer –through the sample or along the boundaries of the sample– can be forced by a convection circuit driven by an air pump [Yah99, Bla00, Pin02, Llo03, Old04, Due04, Alo05, Due07, Pin09a]. Figure 7 shows the evolution of vertical strains (expansive deformations are positive) of compacted bentonite subjected to a reduction in suction (from 150 MPa to 4 MPa) under oedometer conditions (vertical net stress of 10 kPa), using both relative humidity controlled chamber (pure diffusion of vapour) and forced flow of humid air on both ends of the sample. As observed, the forced flow speeds up the process of suction change.

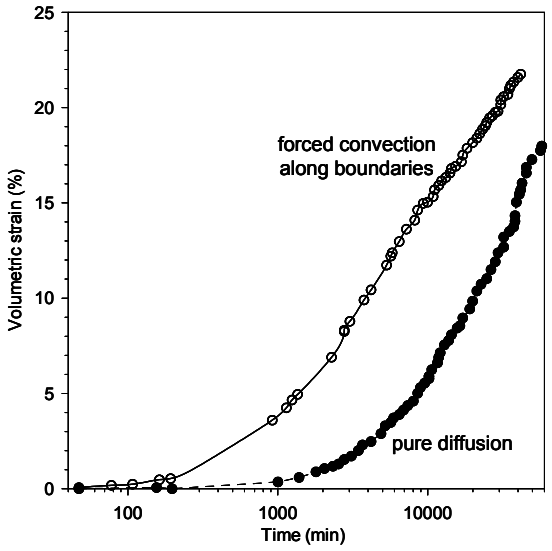

Figure 7: Evolution of volumetric strain (expansion is positive) on compacted bentonite using humid air flow along the boundaries of the sample (forced convection) or controlling the air relative humidity inside a closed chamber (pure diffusion) [Pin09a].

The mass rate transfer of vapour by convection (assuming isothermal conditions and constant dry air pressure u_{da}) can be expressed in terms of vapour density or mixing ratio differences between the reference vessel with aqueous solution (superscript r) and the soil (superscript s) [a: Old04, b: Jot07]

$$\begin{aligned} &\text{a)}\ M_{dry}\frac{\mathrm{d}w}{\mathrm{d}t} = q(\rho_v^r - \rho_v^s) = \frac{q\,M_{mw}}{RT}u_{v0}(h_r^r - h_r^s) \\ &\text{b)}\ M_{dry}\frac{\mathrm{d}w}{\mathrm{d}t} = q_{da}(x^r - x^s) = q_{da}\,x_0(h_r^r - h_r^s) \end{aligned} \qquad (4)$$

where M_{dry} is the soil dry mass, w the gravimetric water content, q the volumetric air flow rate, ρ_v the vapour density in air (water mass per unit volume of air), q_{da} the flow rate of dry air mass, and x the mixing ratio (mass of water vapour per unit mass

of dry air; x_0 represents the saturated mixing ratio). Assuming vapour an ideal gas, the vapour density can be expressed as $\rho_v = M_{mw} u_{v0} h_r / (RT)$, where u_{v0} is the saturated vapour pressure at absolute temperature T, M_{mw} is the molecular mass of water, R is the gas constant, and h_r the relative humidity. Based on the same assumption and that dry air is also an ideal gas, the following expression is obtained $x = M_{mw} u_v / (M_{mda}\, u_{da}) = 0.622\, u_v / u_{da}$, in which M_{mda} is the molecular mass of dry air mixture, u_{da} the dry air pressure and u_v the vapour pressure.

One of the difficulties in using the vapour equilibrium technique is associated with maintaining thermal equilibrium between the reference system (vessel with aqueous solution) and the sample. Assuming that the vapour pressure set by the reference saline solution is also present in the sample, the following correction is proposed, in which h_r is the relative humidity and u_{v0} the saturation vapour pressure at temperature T:

$$h_{r\,sample} = h_{r\,reference} \frac{u_{v0}(T_{reference})}{u_{v0}(T_{sample})} \tag{5}$$

A way to minimise this thermal effect is achieved by disconnecting the reference system that regulates the relative humidity, and allow the equalisation of vapour in the remaining circuit and the soil. This way, the mass of water being transferred from or to the soil is drastically reduced (there is no contribution in water transfer between the vessel and the soil). An equivalent testing procedure was used by [Old04] to overcome the long equalisation periods of the conventional vapour equilibrium technique.

Another problem that comes up when using the forced convection system is associated with air pressure differences created along the circuit. This fact makes that the intended relative humidity applied by the reference vessel cannot be assigned to the remaining circuit and the soil [Pin09a,b]. Dueck [Due04] studied the influence of air pressure changes in a forced convection circuit of vapour –driven by an air pump– and their consequences on the applied relative humidity. Figure 8 shows the experimental setup and the evolution of differential air pressures between two points of the circuit (upstream and downstream the filter stones that transfer vapour to or from the soil). The point upstream the filter is near the reference reservoir ('*ref*' in the figure). On the other hand, the point downstream the filter is close to the aspiration branch of the air pump ('*p*' in the figure) and is subjected to a pressure drop. After vapour equalisation, the pump is turned on and air forced through the circuit. At 67 min the speed of the pump is rapidly increased, and finally reduced from 78 min on. The consequences on the evolution of the relative humidity at the same two points of the circuit are shown in Figure 9. As observed, downstream point '*p*' near the pump undergoes important relative humidity changes due to air pressure drop, while upstream point '*ref*' is buffered by the reference salt solution reservoir. An expression to account for the effects of air pressure variations

on the relative humidity can be proposed based on the assumption that the mixing ratio $x = 0.622\ u_v / u_{da}$ set by the reference salt solution is also set in another point of the constant mass circuit. The following expressions are obtained between the relative humidity reference reservoir $h_{r\,ref}$ set by the salt solution, and another point of the circuit $h_{r\,p}$:

$$u_{v\,p} = u_{vref}\frac{u_{da\,p}}{u_{da\,ref}}$$
$$h_{r\,p} = h_{r\,ref}\frac{u_{da\,p}}{u_{da\,ref}} \tag{6}$$

in which $h_r = u_v / u_{v0}$ is the relative humidity, and u_{v0} is the common saturated vapour pressure.

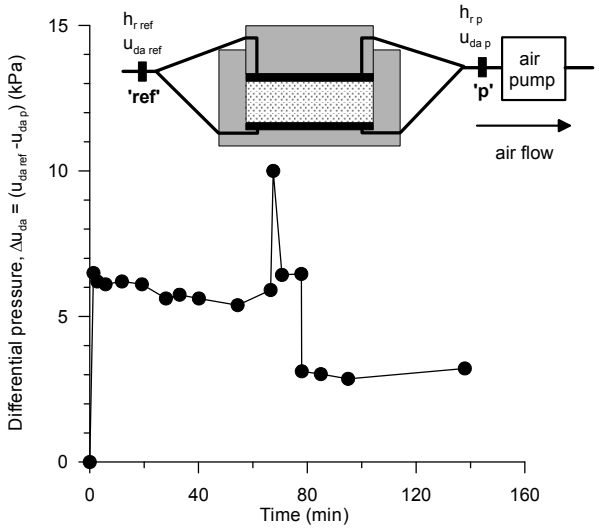

Figure 8: Experimental setup and time evolution of differential air pressures between upstream point 'ref' and downstream point 'p' ([Pin09b], experimental data from [Due04]).

Equation (6) is used to simulate the variations of h_r at downstream point '*p*', $h_{r\,p}$, which are plotted in Figure 9. The absolute pressure at point '*ref*' is fixed at $u_{da\,ref}$ = 101.3 kPa, while absolute pressure changes at point '*p*', $u_{da\,p}$, are estimated from Figure 8: $u_{da\,p}$ = 101.3 kPa-Δu_{da}. If both upstream and downstream absolute pressures are affected: for example, $u_{da\ ref}$ = (101.3+Δu_{da}/2) kPa and $u_{da\,p}$ = (101.3–Δu_{da}/2), equivalent results are obtained. As observed in Figure 9, the simulated points follow the general trend of the measured variations in $h_{r\,p}$, although

they display slightly larger values. An equivalent simulation is used to estimate the relative humidity at upstream point '*ref*', $h_{r\,ref}$, using $h_{r\,p}$ data. In this case, the simulated points do not follow the stable tendency of the relative humidity experimental data, which are buffered by the proximity of the reference salt solution reservoir. Nevertheless, the initial small drop, the next small increase at around 33 min and the smooth peak detected at 67 min are captured in their trend.

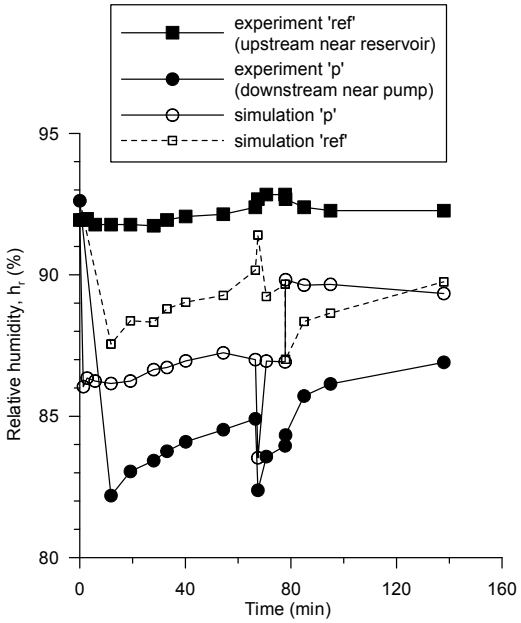

Figure 9. Time evolution of measured and simulated relative humidity at two points of the forced convection circuit: upstream point '*ref*' near the reservoir and downstream point '*p*' close to the pump ([Pin09b, experimental data from [Due04]).

Pintado et al. [Pin09a] performed numerical simulations using Code_Bright [Oli96] to study the physical processes that occur when forcing humid air to flow through a partially saturated sample. It was observed that forcing humid air reduced the equalisation time, but the results from the numerical simulations again highlighted that this flow must be carefully applied to avoid reaching, under steady state conditions, a different total suction than that intended. Gas advective flux followed a generalised Darcy's law with a relative permeability dependent on the degree of saturation. In the numerical analysis, the relationship between the intrinsic permeability for air flow under dry conditions k_{ia} and for water flow under saturated conditions k_{iw} was expressed as $k_{ia} = A k_{iw}$, where A is a material parameter. Due to the uncertainty in the value of parameter A, a back-analysis was done to match the axial deformation measured on densely compacted Febex bentonite during wetting under oedometer conditions (total suction change from 128 MPa to 84 MPa at a constant vertical stress of 0.15 MPa; height of the sample 12 mm). The estimated $A = 3.85\times10^{9}$ was

one order of magnitude higher than the mean value measured in complementary air and water permeability tests, but still within the range of variation of admissible values. As an additional information, the pressure difference between air inlet and outlet ΔP_g=4 kPa was measured when vapour was forced to flow through the specimen. The transient results (time evolution of vertical strains) of the numerical simulations and the fitted experimental results are presented in Figure 10. As clearly observed in the figure, equalisations develop faster at higher pressure differences and higher intrinsic air permeability. An important observation is that final vertical strains are not the same for the four simulations due to the fact that the suction reached at equilibrium is different for all the cases considered. This can be seen in Figure 11, which summarises the different total suctions reached under steady state conditions at the mid-height node of the specimen for the four different cases indicated in Figure 10. If the air pressure difference between the ends of the sample is high, the total suction in the soil under steady state conditions will be different from the expected suction applied by pure diffusion transfer (static test in the figure), as also measured by [Due04, Mer11]. Figure 12 shows that the vapour inflow into the sample decreases with elapsed time because the air permeability becomes lower as the degree of saturation increases during the wetting stage. The mass of vapour that flows into the sample is larger than the mass of vapour that flows out during the transient wetting stage because a percentage of this water is stored in the sample. The steady state is reached after two days, which provides evidence of the efficiency of this experimental method.

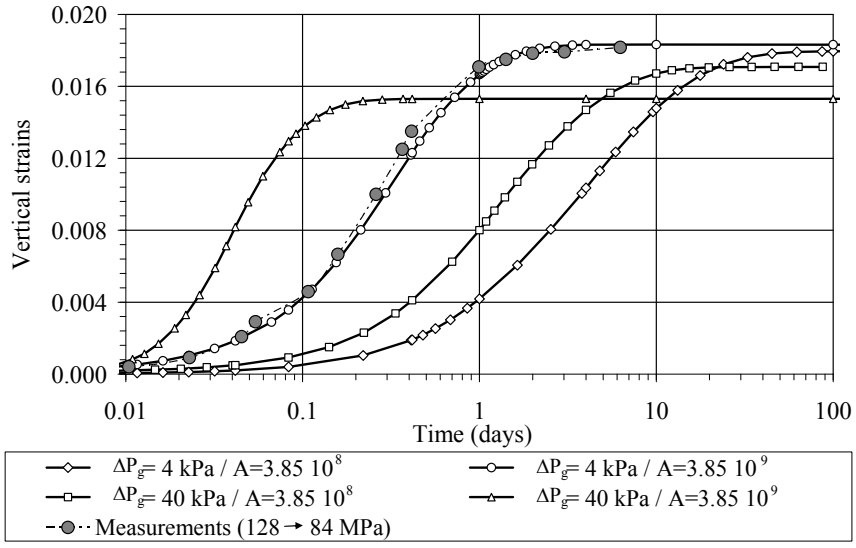

Figure 10: Laboratory measurements and model fitting the evolution of axial strain (swelling is positive) during a wetting path (128 MPa to 84 MPa) at constant vertical net stress (0.15 MPa). Simulations for different A and ΔP_g values [Pin09a].

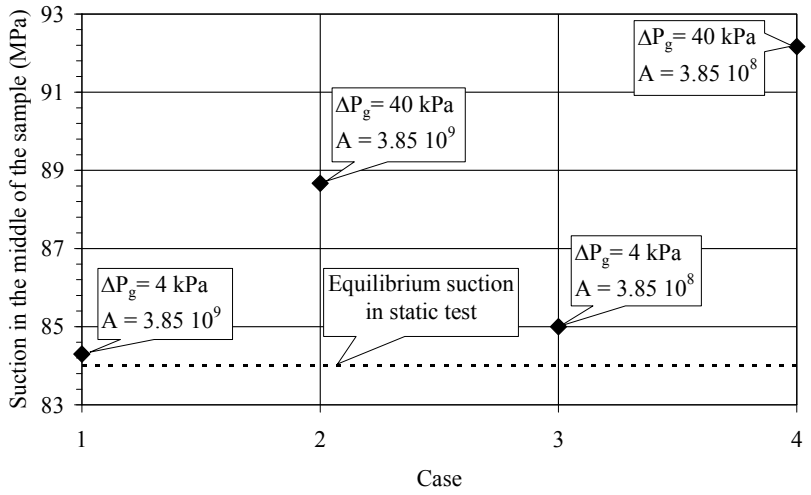

Figure 11: Total suction reached under steady state conditions at the central node of the specimen after the wetting path at constant vertical net stress for the four different cases indicated in Figure 10 [Pin09a].

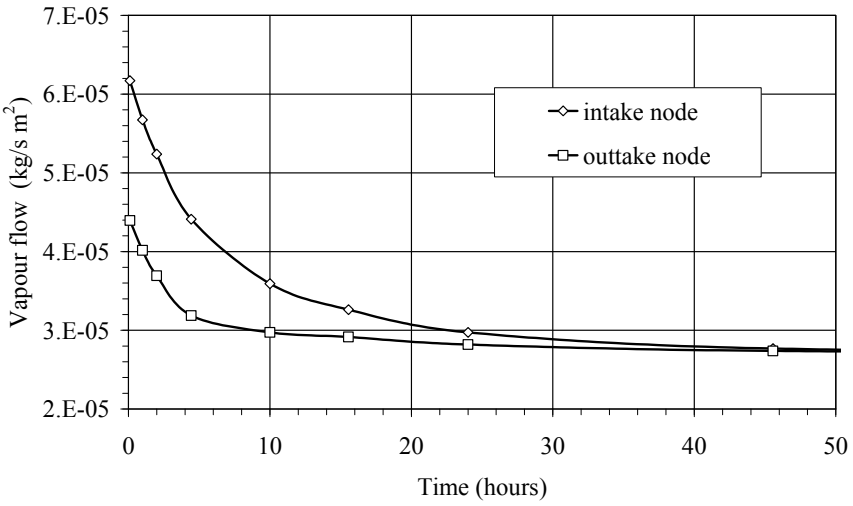

Figure 12: Time evolution of vapour flow during the transient wetting stage. Simulation for A=3.85×109 and ΔP_g=4 kPa [Pin09a].

2.4 Simulation assisted study of the equalisation period when using vapour equilibrium

To analyse the time required for equilibrating homogeneously a deformable sample under oedometer conditions –of major experimental concern when applying a total suction step–, simulation aided techniques (Code_Bright [Oli96]) are presented in this section to study the progression of total suction at local scale and along a drying path (for further details refer to [Mer11]). The usual experimental criterion to define the hydraulic equalisation period under oedometer conditions is based on measuring axial strains and controlling axial strain rates below a specified value (typically below 0.1%/day), due to the experimental difficulty in knowing the precise hydraulic status of the sample during vapour transfer (usually the evolution of vapour transferred to or from the sample is not measured). The two main challenges of the simulations are the correct computation of the evolution of axial strains of the sample during total suction application and to verify if suction stabilises at the elapsed time indicated by the mechanistic approach used conventionally in the experimental procedure (< 0.1%/day).

In the simulation of the results, the flux of water in the gas phase is governed essentially by the non-advective flux, since the gas pressure is maintained under atmospheric conditions. The non-advective component is a function of the diffusion-dispersion tensor and the gradient of mass fraction of water in the gas phase. The water volumetric advective flux is defined by Darcy's law. This flux is affected by the liquid degree of saturation through a relative permeability. The application of the relative humidity at the sample boundaries is set by Equation (7), similar to that used by [Wil94]. In this equation, evaporation arises from the difference between the vapour density at the soil surface ($\rho_g \varpi_g^w$), and the vapour density in the environment $\left(\rho_g \varpi_g^w\right)^0$. Parameter β_g is associated with the turbulent exchange function and depends on the movement of the air above the evaporating surface.

$$j_g^w = \beta_g \left[\rho_g \varpi_g^w - \left(\rho_g \varpi_g^w \right)^0 \right] \tag{7}$$

Values of parameter β_g were obtained by [Pin09a] for conditions prevailing in laboratory with relative humidity control (β_g=2×10^{-3} m/s) and for a closed oedometer cell with circulating vapour (β_g=4×10^{-4} m/s). In the case of the simulation reported by [Mer11], the parameter was obtained by back-analysis leading to a value of β_g=7×10^{-4} m/s, which is of the same order of magnitude than the values found experimentally. This factor can be considered as an impedance factor affecting the efficiency of the system to release the water from the soil.

As previously indicated, the drying path develops volumetric changes on the sample. Therefore, it is necessary to perform the coupled analysis with a simple constitutive model, which takes into account volumetric changes due to total suction or relative

humidity changes besides net vertical stress changes. The selected mechanical constitutive model on monotonic drying was the nonlinear state surface model for partially saturated soils proposed by [Llo85], together with the shear modulus or the Poisson's ratio to define the increments of shear strain.

Figure 13 presents suction equalisation curves (compression is negative) for clayey samples initially prepared at initial water content w_o=34 % and subjected to three different target suctions under oedometer conditions (4.75 mm is the sample height after vertical stress application: 0.1 MPa). These curves show that the rate of shrinkage depends on the total suction change applied to both top and bottom evaporating surfaces. The sample at s=14 MPa (h_r=90%) requires 266 hours to equilibrate, according to the mechanistic criterion (axial strain rate: 0.1%/day). Samples subjected to total suctions of s=58 MPa (h_r=65%) and s=85 MPa (h_r=54%), require 192 and 169 hours, respectively. It is interesting to remark that the sample subjected to the lowest total suction change requires more time to stabilise compared to the remaining ones, despite being closer to the initial saturated state. In this case, suction equalisation time is controlled by the flux of vapour interaction between the sample and the environment, which mainly depends on the vapour density gradient and the exchange properties between the evaporating surface and the glass chamber atmosphere. Results of the simulated curves compared with the experimental ones are plotted in Figure 13.

In Figure 14 the evolutions of total suction at mid-height of the sample for the three simulations are presented. The figure indicates that suction takes around 120 hours to equilibrate for the simulation at s=85 MPa, 168 hours for the simulation at s=58 MPa and 312 hours for the simulation at s=14 MPa. Again and consistent with the mechanistic approach, systematically longer times are required for lower total suctions values. When comparing these simulated equalisation times with the ones based on vertical strain rates, the results indicate that for the lowest suction the experimental time of 266 hours is lower than that given by the simulation. This fact indicates that an additional period of at least 48 hours has to be considered to ensure suction equalisation throughout the sample height. On the other hand, for the remaining applied suctions, the experimental equalisation time given by the mechanistic criterion gives somewhat higher values compared with the numerical observations. Based on these simulations, it appears that the equalisation period based on a mechanical stabilisation criterion (time required to attain vertical strain rates lower than 0.1%/day) is an appropriate way to estimate the suction equalisation period.

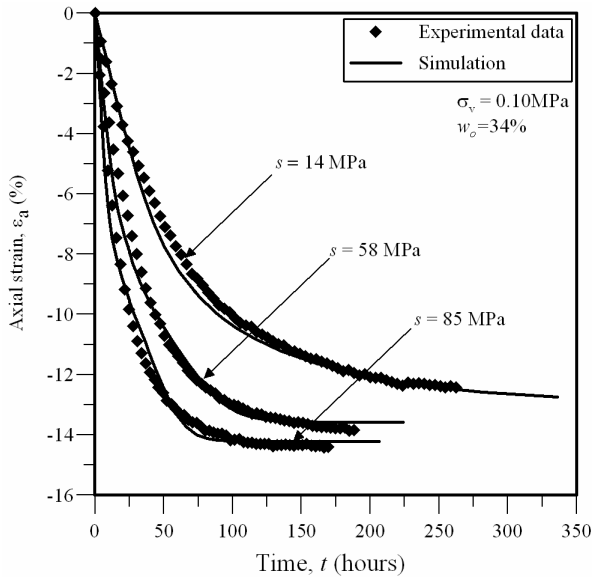

Figure 13: Experimental and simulated axial strain evolutions (compression is negative) for clayey samples subjected to drying at three different target total suctions [Mer11].

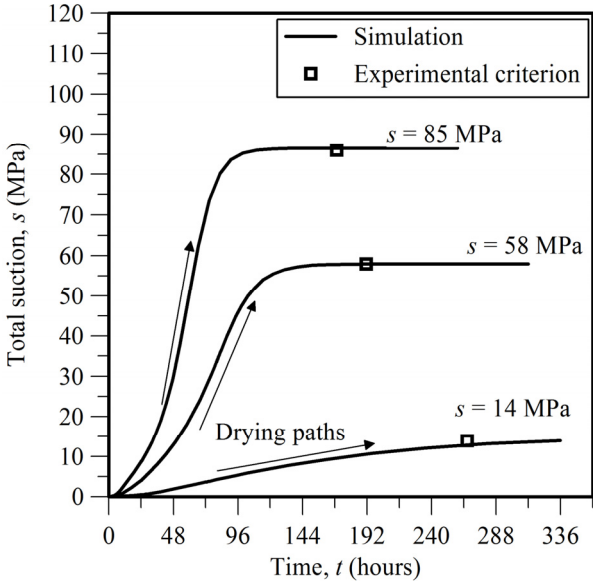

Figure 14: Simulated total suction evolution at mid-height of the sample and comparison with the equalisation time estimated experimentally based on a mechanistic criterion [Mer11].

3 Electro-chemo-hydraulic processes

3.1 Introduction

In the following, electrical and electrochemical processes in geomaterials will be reviewed in light of two possible classes of applications. The first one is electrical characterisation, or the determination of the electrical characteristics (electrical conductivity and impedance) of the medium. Electrical characteristics can be related to the porosity, fabric and saturation degree of the geomaterial and to the properties of the constituent phases, so that the electrical characterisation can contribute to indirect evaluation of porosity, degree of saturation and water salinity. The second class of applications is the induction of transport processes, which can be both direct (such as electromigration, or transport of ions under an electrical field) and coupled (such as electroosmosis, or transport of water within a porous medium under an electrical field). Transport processes induced by an electrical field can be used both for mechanical purposes (consolidation and slope stabilisation) or environmental purposes (remediation of contaminated sites).

3.2 Electrical conductivity of soils and rocks

Electrical flux in geomaterials could be both a direct flux or coupled flux (streaming current, heat current and diffusion current, see following paragraph and [Mit05]). When no hydraulic, thermal and chemical gradients are acting, or for negligible coupling coefficients, electrical current density i is proportional to the gradient of the electrical potential ϕ as according to Ohm's law:

$$i = -\chi_t \nabla \phi \tag{8}$$

where χ_t [1] is the electrical conductivity of the soil and ϕ is the electrical potential.

In theory, electrical charges could travel through the solid phase, the water phase and at the interface between water and solid phase (surface conduction), while practically no electrical flux occurs in air or hydrocarbons. Most minerals are insulators (although the electrical conductivity of metals can be as high as $10^5 - 10^8$ S/m) and their contribution to the electrical conductivity of the geomaterial is usually neglected: readers interested in the analysis and interpretation of the electrical behaviour of dry rocks can refer to the book of [Par67].

Several theoretical and empirical relationships have been proposed to model the electrical conductivity of geomaterials. These relationships take into account the

[1] The usual symbol for electrical conductivity is σ. Here χ is used instead to avoid confusion with stress.

effects of tortuosity, particle shape, degree of saturation, microstructure and surface conductivity in different ways[2].

Among the relationships that do not consider surface conductivity, Archie's law [Arc42] is the most widely used. It has been derived for oil reservoir sands, and accounts for the effects of porosity and saturation as follows:

$$\chi_t = \chi_w n^m S_r^{\ p} \tag{9}$$

where χ_w is the electrical conductivity of the water phase, n is the porosity, m is an exponent that accounts for the tortuosity of the porous medium, S_r is the degree of saturation and p is an empirical exponent that also depends on the fabric of the material (particularly on its pore size distribution, see e.g. [Sen97]). The formation factor F^*:

$$F^* = n^{-m} \tag{10}$$

often used in oil engineering represents the ratio of the resistivity of the saturated material to the resistivity of the saturating water.

Archie's law in saturated conditions has been extended to account for surface conductivity by [Wax68]:

$$\chi_t = X\left(\chi_w + \chi_s\right) \tag{11}$$

where X is a constant analogous to $(F^*)^{-1}$ and χ_s is a surface conductivity term. A limitation of Waxman and Smits expression (11) is that it assumes that the surface conductivity is affected by the geometry of the porous medium in the same way as the water conductivity term. This expression should be used with caution also because surface conductivity is not constant for a given material, but depends on the characteristics of the solid phase surface groups, on the pore fluid pH and on its concentration (for a detailed discussion see [Del05]). As a matter of fact, surface conductivity is an important contribution for clayey soils with a high specific surface: its value is greater the lower the salinity of the pore water. In these particular soils, attention must be paid to the fact that chemistry also influences the dimensions of pores [e.g. Mus03] and then affects the soil electrical conductivity by altering the formation factor. A discussion on aspects related to surface conductivity, including simple theoretical models to evaluate surface conductivity starting from the Diffuse Double Layer theory, can be found in [Kle03].

[2] For a list of theoretical models, the book of [San01] is suggested.

3.3 Electrolytic conduction

In water the electrical current is carried by ions, dragged towards the electrodes of opposite polarity. Ionic mobility u is the drift velocity of an ion under an unit electric field. According to the Nernst-Einstein equation, at infinite dilution the ionic mobility is proportional to the diffusion coefficient D:

$$u = \frac{D\nu F}{RT} \tag{12}$$

where ν is stoichiometric coefficient of the ion, F is Faraday's constant (F = 96485 C/mol of electrons), R is universal gas constant (8.314 Joule mol^{-1} K^{-1}) and T is absolute temperature. Contribution of ions of a given specie i to the electrical conductivity of a solution is:

$$\chi_i = c_i u_i \nu_i F = c_i \Lambda_i \tag{13}$$

where c_i is concentration (expressed in mol/m^3) and Λ_i is molar conductivity (electrical conductivity of a mole) of the specie i (expressed in $S\,m^2$/mol). The overall electrical conductivity of a water solution is then given by the sum of the contributions of the n species in solution:

$$\chi_w = F \sum_{i=1}^{n} c_i \nu_i u_i \tag{14}$$

Equation (14) shows that χ_w is related to the concentration of dissolved species. The actual relationship depends on concentration. At high concentrations, ionic mobility and molar conductivity decrease, and the linearity between concentration and electrical conductivity is lost. Figure 15 shows experimental results and interpretation of measurements of electrical conductivity at increasing concentrations of NaCl electrolyte (see also [Kle03]).

3.4 Electrolytic cells and electrode reactions

It is of interest to understand how electrical current is transmitted to a water solution, since this process involves electrode reactions, *electrolysis,* that can change the chemical composition of the pore water at the points of injection.

An electrolyte, or a ionic conductor, is a substance where ions are the main charge carriers. Two electrodes injecting a current and the electrolyte between them constitute an *electrolytic cell.* The interface between the electrodes and the electrolyte is the seat of chemical reactions necessary to exchange electrons between the metallic part of the circuit (where electrons are the charge carriers) and the electrolyte (where

ions are the charge carriers). A conceptual scheme of transport and reactions processes occurring is given in Figure 16.

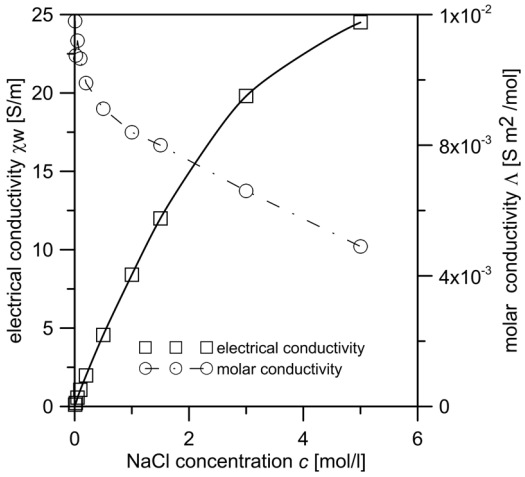

Figure 15: Electrical conductivity and molar conductivity of NaCl solutions (modified from [Mus05]).

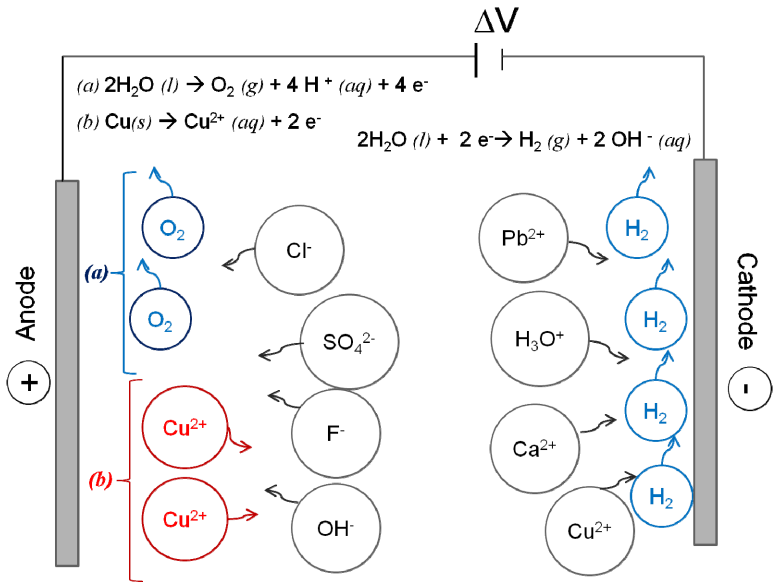

Figure 16: Conceptual scheme of transport and reactions within an electrolytic cell.

Electrons are removed from the electrolyte through an oxidation reaction. One or more species in the electrolyte serve as electron donor (*reductant*) and the electrode as a receiver of electrons. Oxidation reactions are written as follows:

$$\mathrm{Red}_1 \rightarrow \mathrm{Ox}_1 + \nu \mathrm{e}^- \tag{15}$$

where *Red* is the reductant specie, *Ox* the oxidant and ν is the stoichiometric coefficient of the electrons e^- involved in the reaction. The electrode at which oxidation occurs is the *anode*: in an electrolytic cell this is the positive electrode (the one towards which are attracted ions with negative charge, *anions*).

Electrons travel through the external metallic circuit and re-enter the cell at the opposite electrode, the *cathode* by means of a reduction reaction:

$$\mathrm{Ox}_2 + \nu \mathrm{e}^- \rightarrow \mathrm{Red}_2 \tag{16}$$

In an electrolytic cell the cathode is the negative electrode: it attracts *cations* (species with positive charge).

Considering that many species are dissolved in the pore water of a soil, one could imagine several different possible redox reactions. Actually, only a few of them (ideally one oxidation and one reduction reaction) do occur. If the material constituting the electrodes and the species in solution are known, it is possible to foresee which reactions will take place on basis of the electrochemical potential *E*. This is evaluated on basis of the Nernst equation (17), and it is a function of the standard potential of the reaction E^0, of absolute temperature and of stoichiometric coefficient:

$$E = E^0 - \frac{RT}{\nu F} \ln \frac{a_{red}}{a_{ox}} \tag{17}$$

where a_{red} and a_{ox} are the activities of the reduced and oxidised specie.

Standard potentials can be found in chemistry textbooks [Atk10]. The reference reaction is reduction of protons, whose standard potential E^0 is conventionally zero:

$$2H^+ + 2e^- \rightarrow H_2 \tag{18}$$

At the anode the reaction with the most negative (or least positive) potential is favoured until the species involved are used up and/or until a high voltage stimulates competing reactions. Depending on the material used to build the electrode, M_A, the oxidation reaction (15) can either be oxidation of water [Loc83]:

$$2H_2O(l) \rightarrow O_2(g) + 4H^+(aq) + 4e^- \tag{19a}$$

which has a standard potential $E^0 = +1.23\ V$ ($E = +0.82\ V$ when pH = 7), or oxidation of the electrode:

$$M_A \rightarrow M_A^{v+} + ve^- \tag{19b}$$

As it can be appreciated in Table 1, the standard electrode potential of the reaction (19a) is higher than that of some typical metals that could be used to build the electrodes (Aluminium, Iron or Copper), but is smaller than that of noble metals (Platinum or Gold).

Table 1: Selected standard potentials of reduction reactions.

Reaction	**Standard Electrode Potential E^0 (V)**	**Reaction**	**Standard Electrode Potential E^0 (V)**
$Al^{3+} + 3e^- \rightleftharpoons Al(s)$	−1.660	$2H_2O\ (l) \rightleftharpoons O_2(g) + 4H^+(aq) + 4e^-$	+1.230 +0.82 (pH = 7)
$Zn^{2+} + 2e^- \rightleftharpoons Zn(s)$	−0.762	$Hg^{2+} + 2e^- \rightleftharpoons Hg(l)$	+0.850
$Fe^{2+} + 2e^- \rightleftharpoons Fe(s)$	−0.440	$Pt^{2+} + 2e^- \rightleftharpoons Pt(s)$	+1.188
$Cu^{2+} + 2e^- \rightleftharpoons Cu(s)$	+0.340	$Au^+ + e^- \rightleftharpoons Au(s)$	+1.690

Anodes made of Aluminium, Zinc, Iron or Copper in a neutral water environment release the metallic cation into the electrolyte (e.g. a Copper electrodes will enrich the electrolyte with Cu^{2+} ions) and corrode (case *(b)* in Figure 16). Anodes made of inert materials (e.g. graphite) or made of noble metals do not corrode, and reaction (19a) takes place since potential E is lower than the metal's one. In this case, water next to the anode acidifies and oxygen is released in gaseous form (case *(a)* in Figure 16).

At the cathode the reaction with the most positive potential is favoured. Water reduction:

$$2H_2O(l) + 2e^- \rightarrow H_2(g) + 2OH^- \tag{20}$$

often occurs since its electrochemical potential at pH = 7 is E = + 0.41 V, which is higher than most potentials of reactions involving metal cations.

The mass q of elements altered by electrolytic reactions (e.g. the mass of H^+ or OH^- ions developed when using inert electrodes) can be calculated through Faraday's laws of electrolysis:

$$q = \frac{Q}{F} \cdot \frac{M}{\nu} \tag{21}$$

where Q is cumulate electrical charge passing through the cell (expressed in Coulombs, C) and M is molar mass of the substance.

3.5 Electrode polarisation and overpotential phenomena

Compensation of electrical charges at the electrode – electrolyte interface causes polarisation, which is the development of an electrical double layer consisting of a sheet of positive charge at the surface of the electrode and a sheet of negative charge next to it in the solution (or vice versa). The electrical double layer makes the electrical potential of the solution different from the electrical potential of the electrode. Theoretical models have been formulated describing the concentration of counterions in the solution and the associated voltage profile (Helmholtz layer model, Gouy-Chapman model, Stern model) (see [Mit05]).

The difference between the electrical potential of the electrode and the electrical potential of the solution next to it does not only depend on polarisation, but also on metal deposition, gas development and on the intensity of the electrical current. Altogether, this difference is called *overpotential* η. The exact value of the overpotential is difficult to predict theoretically, although significant deposition / gas development is expected to occur only when $\eta > 0.6$ V [Atk10].

3.6 Electrical conductivity measurements

The simplest way to determine the electrical conductivity χ of a specimen in laboratory is by measuring the electrical resistance R in a given geometrical arrangement. R is obtained through Ohm's law:

$$\Delta\phi = R \cdot I \tag{22}$$

where $\Delta\phi$ is electrical potential drop between two points and I is electrical current. Once that R is known, χ is derived through a shape factor α:

$$\chi = \frac{1}{\rho} = \frac{\alpha}{R} \tag{23}$$

For instance, if R is the resistance of a parallelepiped under one dimensional flux condition, it is:

$$\chi = \frac{1}{\rho} = \frac{l}{RA} \tag{24}$$

where ρ is the resistivity (inverse of conductivity), l is the distance between the points where the electrical potential is measured and A is the section of the sample. From Equation (24) it follows that the shape factor in one dimensional flow conditions is $\alpha = l/A$.

Two different types of experimental setup are used to determine the electrical conductivity of soil and rock samples: the two terminal electrodes and the four terminal electrodes systems (Figure 17). In the two terminal electrodes system, the anode and the cathode are used both to inject the electrical current I and to measure the electrical potential drop $\Delta\phi$.

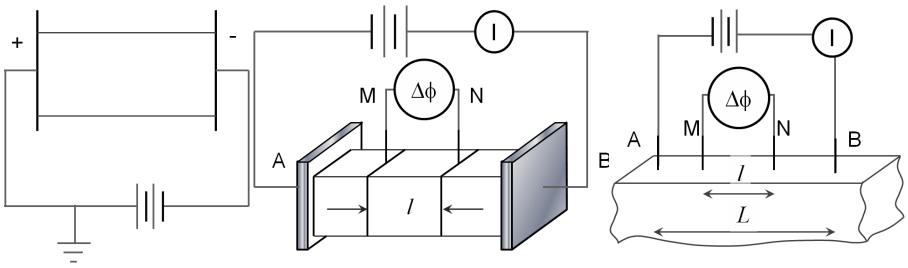

Figure 17: Two electrodes terminal (left) and four electrodes terminal (center and right) systems (modified from [Par67])

Although very simple to build, this system presents the disadvantage that the potential drop measured between the cathode and the anode necessarily includes the overpotential η, whose value is in principle unknown. Very high η are expected when inert electrodes are used, since O_2 and H_2 bubbles produced by electrolysis of water accumulate at the electrode – specimen interface, acting as very powerful insulators. Overpotential is expected to reduce at increasing frequency of the electrical signal: electrical potential drops measured with a two electrodes system at relatively high frequencies are in principle related only to the resistance of the soil specimen. Measurements performed by a two electrodes system are anyway difficult to interpret, since the frequency above which polarisation effects becomes negligible (limiting frequency) depends on conductivity, permittivity, and length of the specimen [Kle97]. On basis of permittivity measurements, Klein and Santamarina [Kle97] found that the limiting frequency of sands and kaolinite specimens at different water

contents and water salinity ranged between 10^2 and 10^4 Hz, although real conductivity values appeared to be insensitive of frequency above 100 Hz. More critical evidences were obtained for bentonite samples, where the limiting frequency in terms of permittivity ranged as high as 1 MHz and conductivity values were frequency dependent for $f < 1$ kHz.

In the four electrodes measurement system, two electrodes (A and B) are devoted to inject the electrical current and two other electrodes (M and N) are devoted to measure the potential drop: this excludes overpotential effects. Anyway, since also these electrodes work over a metal – electrolyte interface, they measure an overall electrochemical potential difference $\Delta\psi$ and not simply the electrical potential difference, $\Delta\phi$. Their readings can then be partially affected by differences in concentration of the species in solution. To keep errors to a minimum, it is suggested to use well referenced electrodes jointly with solutions whose composition and expected concentration is, although broadly, anticipated. For instance, [Mus00] used silver chloride electrodes (Figure 18) to monitor the local evolution of the electrical conductivity within clay samples during bench scale electrokinetic tests. The working principle is the silver – silver chloride redox reaction:

$$Ag_{(s)} + Cl^- \rightleftarrows AgCl_{(s)} + e^- \tag{25}$$

AgCl salt deposits at the interface between silver and the electrolyte (Figure 18), centre): since the only species in solution is the chloride anion, the Nernst equation (17) of reaction (25) is:

$$E = E^0 - \frac{RT}{F} \ln a_{Cl^-} \tag{26}$$

When two silver chloride electrodes are used (M and N) the measured potential difference is then:

$$\Delta\psi = \Delta\phi - \frac{RT}{F} \ln\left(\frac{a_{cl^-}^M}{a_{cl^-}^N}\right) \tag{27}$$

where $a_{Cl^-}{}^{(M)}$ and $a_{Cl^-}{}^{(N)}$ are activity of the chloride in the proximity of electrode M and N. By using silver electrode measurements without corrections (then using $\Delta\psi$ instead of $\Delta\phi$), the error made is 0.06 V when $a_{Cl^-}{}^{(M)} / a_{Cl^-}{}^{(N)} = 10$, and is 0.12 V when $a_{Cl^-}{}^{(M)} / a_{Cl^-}{}^{(N)} = 100$.

3.7 Review of laboratory experiments involving electrical conductivity measurements

Most two electrodes terminal systems described in the literature have two cylindrical electrodes laying on top and bottom of soil samples. Samples are inserted into cylinders of non-conductive materials. Some of these cells allow a vertical load to be applied, so they also work as oedometer cells. Materials used for the electrodes include rigid metals (e.g. copper, aluminium, steel), noble metals that do not oxidize (platinum, gold) and graphite (when porous, it can also work as a porous stone).

Table 2 presents a schematic review of selected studies taken from the geomechanical literature where two electrodes terminal systems were used.

Table 2: Selected studies with two electrodes terminal systems.

Study	Electrodes/ Geometry	Mechanical	Hydraulic / Chemical	Objective / Results
[Fuk99]	Stainless steel mesh 1D vertical meas.	Oedometer	-	Evolution of microstructure with load in undisturbed and reconstituted clay specimens
[McC05]	Stainless steel. 1D horizontal and vertical measurement	Oedometer	-	Evaluation of anisotropy upon loading of undisturbed and reconstituted samples
[Lee08]	Stainless steel. Quasi spherical (Needle probe)	Oedometer	-	Evolution of resistance evolution upon loading: evidences of anisotropy and load history effects
[Fuk01]	Stainless steel mesh 1D vertical measurements	Oedometer	Imposed saturation degree / pore water salinity	Preliminary characterisation of soil electrical behaviour aimed at using a four electrodes electrical CPT for the detection of contaminated layers.
[Ble03]	Stainless steel. 1D radial and vertical measurements	-	1 D diffusion in column and oedometer	Evaluation of the effective diffusion parameter of NaCl in kaolin specimens
[Bez09]	Stainless steel. 1D radial measurements	-	1 D diffusion in column	Evaluation of the effective diffusion parameter of NaCl in kaolin specimens
[Att08]	Silver Paint. 1D vertical measurements	-	Evaporation	Evidencing differences between water retention and electrical conductivity in the unsaturated range
[Cho04]	Quasi spherical (Needle probe)	-	-	Evaluation of specimen heterogeneity through electrical resistance profiles
[Fes07]	Stainless steel. Quasi spherical (Needle probe)	-	-	Evaluation of specimen heterogeneity through electrical resistance profiles
[Mus09]	Stainless steel. Quasi spherical (Needle probe)	-	Evaporation	Evaluation of local saturation degree through electrical resistance profiles

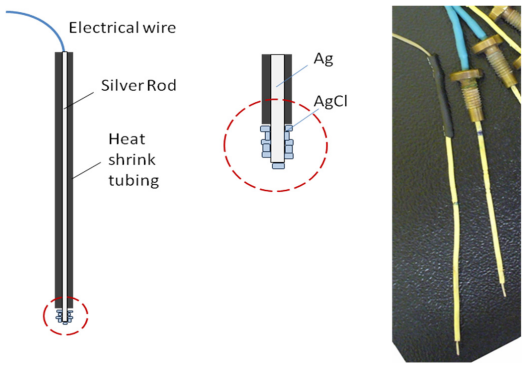

Figure 18: Scheme of a silver chloride electrode for voltage measurements (left), detail of the Ag/AgCl interface (centre), picture of two silver chloride electrodes (right).

Results of two electrode terminals systems were checked against four electrodes terminal systems by [Kle97], suggesting the possibility of explicitly taking into account overpotential effects in the circuit analysis of the experimental results. They proposed a 'simple circuit', introducing an electrode capacitance C_e (Figure 19, left), and an 'enhanced circuit', introducing an electrode capacitance C_e in parallel with an electrode resistance R_e and a ionic diffusion term Q (Figure 19 right).

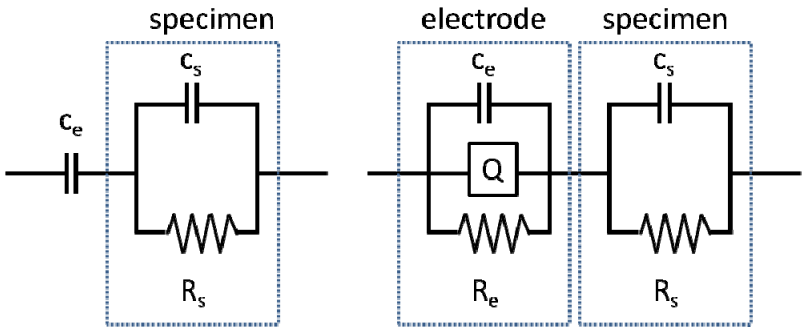

Figure 19: Simple (left) and enhanced (right) circuits for the interpretation of 2 electrode terminals systems. Modified from [Kle97].

Four electrodes terminal systems have been implemented in different geometries. In some studies (e.g. [Abu96a,b]) electrodes A and B are plates at the sample top and bottom and electrodes M and N are punctual electrodes (rods) between A and B, so that one dimensional electrical flow occurs (as in the centre of Figure 17). In many other studies all electrodes are punctual and disposed in different geometries at the sample boundaries, as in the right side of Figure 17 (e.g. [Mou67, Kal93]).

Table 3: Selected studies with four electrodes terminal systems.

Study	Eletrodes / Geometry	Mechanical	Hydraulic / Chemical	Objective / Results
[Mou67]	6 punctual platinum electrodes / 2 pairs of injecting electrodes at the base, 1 pair of voltage electrodes at the top	Oedometer	-	Evaluation of transversally isotropic parameters for electrical anisotropy. 1.10 (a) < χ_h / χ_v < 25.5 (b) a): packed dry bentonite, σ_v = 55 kPa b): bentonite slurry, distilled water, σ_v =165 kPa
[Ana95]	4 punctual circular electrodes / 3 on the base and 1 on the top	Oedometer	-	Evaluation of electrical anisotropy during oedometer loading.
[Kug96]	4 punctual circular electrodes / 3 on the base and 1 on the top	Triaxial	-	Evaluation of electrical anisotropy during triaxial shearing of kaolinite samples
[Kal93]	8 punctual electrodes/ work in turn 4 at a time: 2 external inject current, 2 internal measure potential	-	Water content imposed with pressure plate	Evaluation of relationship between water content and electrical conductivity. Estimation of surface conductivity.
[Abu96a]	2 copper plates and 2 copper rods / vertical measurements: plates inject current, rods measure potential	-	water content imposed upon standard proctor compaction	Evaluation of relationship between water content and electrical conductivity of compacted samples. Loose agreement between electrical conductivity and hydraulic permeability
[Abu96b]	2 copper plates and 2 copper rods / vertical measurements: plates inject current, rods measure potential			Evaluation of bentonite content in sand - bentonite mixtures

As it can be appreciated in Tables 2 and 3, electrical measurements have been associated to an equal number of hydro-chemical and mechanical studies. In studies related to mechanical processes, electrical measurements mostly provided semi quantitative information, such as the anisotropy ratio $A = \chi_h / \chi_v$ used in [Ana95] and [Kug96] to provide an insight on microstructure evolution and on its effects during loading of clay samples in oedometer and triaxial conditions (where χ_h is the horizontal component and χ_v is the vertical component of the electrical conductivity tensor). In other studies, good results were obtained in terms of indirect evaluation of transport parameters ([Ble03]). To allow this interpretation, electrical measurements have to be interpreted in terms of evolution of concentration of a species in space and time. Transport models are then used to simulate the hydro-chemical processes, and transport parameters are sought by means of optimisation through back analyses. Several measurements have to be taken: a limitation of most of the experimental set ups presented in Tables 2 and 3 is that they consider the volume of soil between the measuring electrodes as homogeneous, limiting the possibility of studying transport processes.

A way to relax the assumption of homogeneity comes from performing an high number of electrical measurements with different electrodes in different parts of the

specimen, to be integrated by means of tomography reconstructions (ERT technique, discussed in the previous chapter). Another possibility is moving the measuring electrodes along the specimen. This has been implemented as an electrical needle probe in [Cho04]. The probe is a two terminal electrode system made of two coaxial electrodes: the first one (internal) is a rod, the second one (external) is a metallic hollow cylinder (Figure 20a). The two electrodes are separated by a dielectric material and the electrical signal between them must travel entirely in the soil. The needle probe can be inserted and moved into the soil sample to gather an electrical profile. To be effective, electrical profiling must be done without locally affecting porosity (e.g. in undrained conditions).

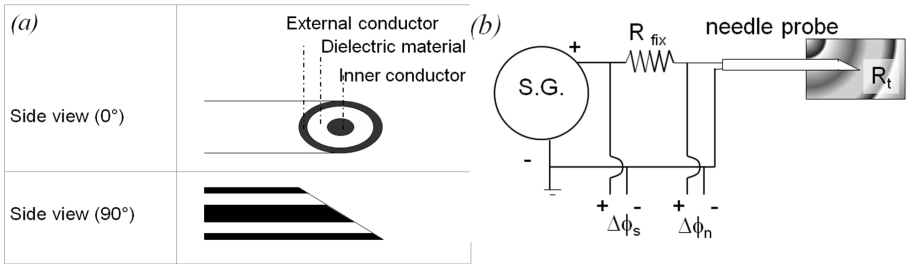

Figure 20: Scheme of the needle probe: arrangement of the electrodes (left), simplified electrical circuit with signal generator and needle probe (right) (modified from [Cho04]).

A scheme of the electrical circuit of [Cho04] is given in Figure 20b. A known fixed resistance R_{fix} is in series with the probe and the electrical current in the circuit is:

$$I = \frac{\Delta\phi_s - \Delta\phi_n}{R_{fix}} \tag{28}$$

where $\Delta\phi_s$ is the potential drop imposed by the signal generator over the whole circuit and $\Delta\phi_n$. is the potential drop in correspondence of the probe. The electrical resistance R of the investigated soil volume is then:

$$R = \frac{\Delta\phi_n}{I} \tag{29}$$

Calibration requires that the effects of frequency on measurements are taken into account. First an operating frequency, higher than the limiting one, is chosen. Then resistance measurements are taken at known medium resistivity, a procedure that is implemented by measuring R values immersing the probe into different solutions having known values of ρ. Experimental (R, ρ) couples are then fitted to determine

the shape factor α of Equation (23): Figure 21a shows a calibration of a needle probe taken from [Fes07]. This relationship is then inverted when interpreting experimental data to evaluate the soil electrical conductivity on base of resistance measurements.

Figure 21b, modified from [Fes07], shows an application of electrical profiles provided by the needle probe, interpreted in terms of porosity. It refers to measurements taken along a column after sedimentation of a dry clay material (Beaucaire clay) had occurred in water. First the electrical conductivity of the water, χ_w, was measured in the supernatant. Local values of soil conductivity χ_t were then estimated based on resistance measurements, through the calibration of Figure 21a. The profile of porosity was then obtained inverting Archie's relationship (9) for the saturated case:

$$n = \left(\frac{\chi_t}{\chi_w} \right)^{1/m} \tag{30}$$

where it was assumed that m = 1.8. Estimated porosities were consistent with direct measurements, based on local mass measurements, proving the potentialities of this approach.

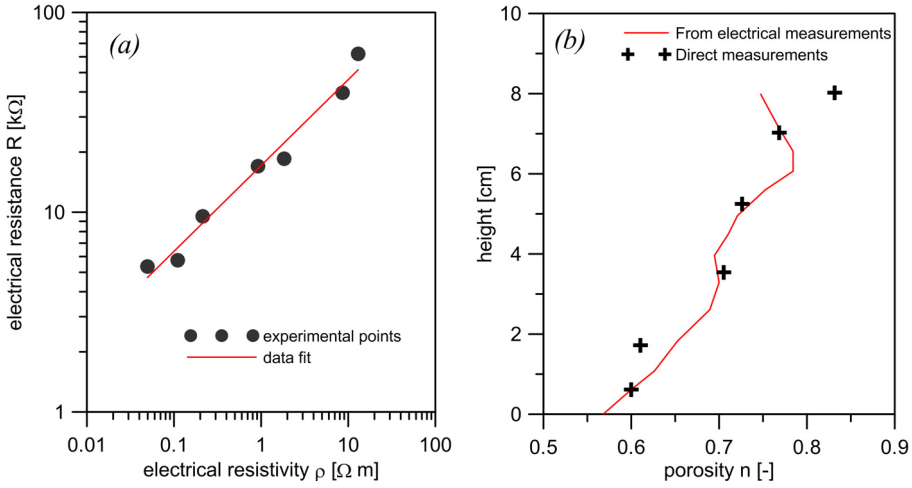

Figure 21: Calibration curve of an electrical needle probe (a) and porosity profile of a column of a sedimented clay obtained with needle probe measurements (b) (modified from [Fes07]).

3.8 Coupled effects of electro-hydraulic fields: electroosmosis

Direct flows discussed in detail in the previous sections are not exhaustive of the processes which are promoted in the presence of field gradients. To close this chapter it is worth mentioning, although briefly, electroosmosis (already introduced in Section 3), which is the transport of water induced by an electric field.

Electroosmosis is an inherently coupled electro-hydraulic process, promoted by the unbalanced surface charge of the solid grains [Spo84]. This coupled flow has been described by means of a number of chemo-physically based models at the pore scale, which justify the formulation of phenomenological laws adopted in geotechnical engineering.

With reference to saturated conditions, the simplest phenomenological formulation for coupled hydro-electrical fluxes in saturated soils is given by the linear system [Mit05]:

$$\begin{bmatrix} i \\ j_w \end{bmatrix} = -\begin{bmatrix} \chi_t & \varepsilon^* \\ k_{eo} & k_w \end{bmatrix} \begin{bmatrix} \nabla\phi \\ \nabla h_w \end{bmatrix} \tag{31}$$

where i is the current density, j_w is the volumetric discharge of water per unit area, $\nabla\phi$ is the electrical potential gradient, ∇h_w is the hydraulic head gradient. The electrical conductivity, χ_t, and the hydraulic conductivity, k_w, account for direct fluxes. The out-of-diagonal coefficients respectively quantify mass flow promoted by the electric field, through the electroosmotic permeability, k_{eo}, and for electric current arising as a consequence of mass flow of water, through the coefficient ε^*. The latter coefficient, describing the so-called *streaming potential* can be derived from the electroosmotic permeability by means of the Onsager's reciprocity principle, and it will not be further taken into consideration in the following. It is worth noting that, for practical applications, which will be briefly discussed in another chapter, the streaming potential can be usually disregarded.

Here the attention is focused on the limits of this linear formulation in the light of the considerations made in the previous sections on the chemical processes which accompany an electric field in the soil.

Relying on the linear formulation given by Equation (31), the electroosmotic permeability could be determined in principle by a very simple experimental setup. A cylindrical cell with insulating and water tight lateral walls could be equipped with a top and bottom plates acting as a pair of electrodes in contact with the sample and allowing for drainage. By imposing the same hydraulic head (and chemical composition) at the boundaries of the sample and constant electrical potential difference between the two plates, a one-dimensional, constant water discharge should be in-

duced. A constant electrical current density is expected in this one-dimensional constant electrical field:

$$\begin{aligned} j_w &= -k_{eo}\,\nabla\phi \\ i &= -\chi_t\,\nabla\phi \end{aligned} \tag{32}$$

Similar experimental arrangement has been adopted extensively in the past to determine the electroosmotic premeability of soils, sometimes in conjunction with uniaxial loading ram to impose vertical stress. In the latter case, the equipment is commonly named *electroosmotic oedometer*. From the electrical point of view, this kind of apparatus belongs to the class of the two electrodes terminal systems, summarised in Table 2. An ideal scheme of such an experimental setup is reported in Figure 22, where the theoretical distributions of pore water pressure and of the electrical potential are indicated.

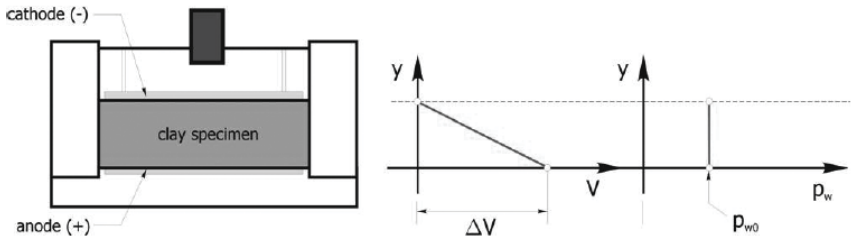

Figure 22: Ideal scheme of electroosmotic oedometer [Tam10].

Selected results from electroosmotic tests performed in a similar equipment are presented in Figures 23 and 24. The comprehensive set of experimental data, together with a detailed description of the equipment developed, and of the material tested are reported in [Gab08a,b] and [Tam10].

In Figure 23 data of water discharge in time are reported of tests lasting not more of 20 minutes at constant applied electric gradient. Water outflow is fairly linear in time although a slight tendency to decrease can be appreciated, even in this short duration tests. If the outflow rate is reported as a function of the applied electrical gradient (Figure 24), a linear relationship between voltage and water flow rate can be drawn and a representative value of the short-term electroosmotic conductivity can be determined.

The data presented in Figure 24 also show the evidence of the energy consumed at the electrodes for water oxidation (section 3.4) and the occurrence of an overpotential η (section 3.5). The outflow rate of water leaving the sample is in fact found to grow linearly with the applied potential drop, if an offset of 1.44 V is applied. This offset can be associated to overpotential effects: since it *consumes* a portion of the

electrical potential, not all the gross potential applied is available as a source for coupled fluxes, and only a part of it being actually imposed on the soil sample. As already discussed in section 3.6, the electrical overpotential, may be due to different and concurrent causes.

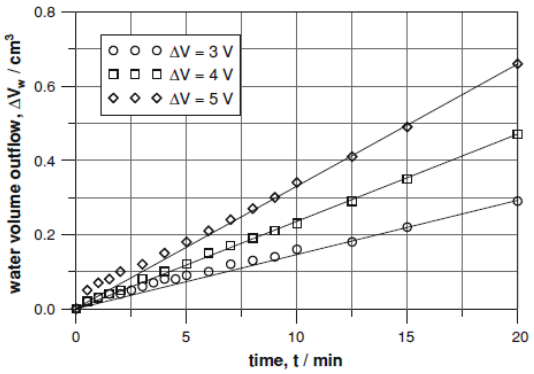

Figure 23: Water discharge data of short term electroosmotic test on a clayey silt [Gab08a].

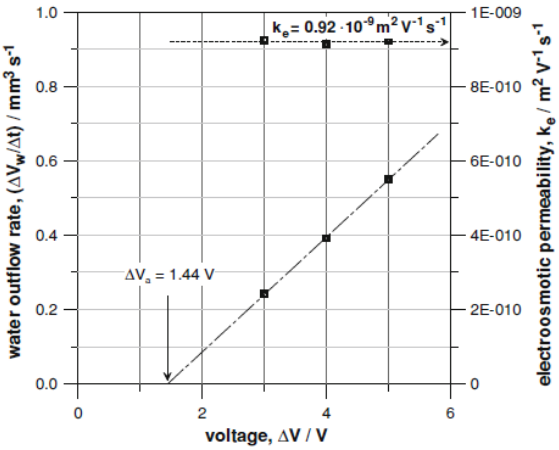

Figure 24: Electroosmotic permeability from data of short term electrokinetic filtration test on a clayey silt [Gab08a].

Results of a similar test, but having longer duration, run on a silty clay of comparable chemical composition as the previous clayey silt, are reported in Figure 25. The test lasted about 15 days, and it was run by imposing a constant current density through the soil, while measuring the voltage at the two extremes of the sample. Dramatic decrease of the average electroosmotic permeability may be observed in

time in the long duration test, which suggests that different coupled phenomena, other than those already described, start to occur in time. Many of these phenomena, discussed in detail in a following section, are actually triggered by local variations of electrical conductivity, due both to variation in the chemical composition of the pore fluid (for example caused by redox reactions, equations (19) and (20)) and by desaturation processes.

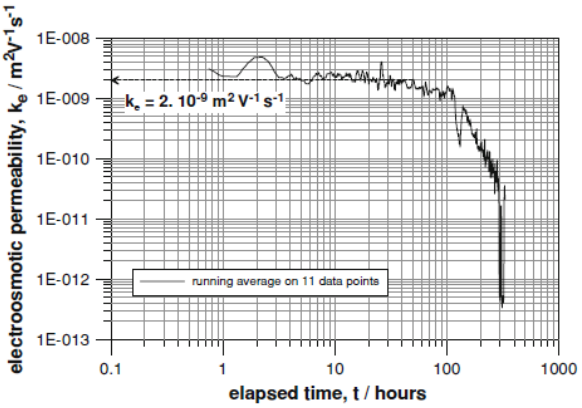

Figure 25: Time evolution of the average electroosmotic permeability of a silty clay in a controlled current density one-dimensional test [Gab08b].

A relevant role has been recognised to be played by penetration into the sample of the gas front generated at the anode [Tam10, Gab08a, Air09], which cannot escape easily from the soil, as it remains entrapped by the water flow towards the cathode. Penetration of the gas front partly desaturates the soil, lowering the electrical conductivity (section 3.2), as well as the electroosmotic permeability.

Little experimental information is available in the literature to quantify the influence of the water degree of saturation on the electroosmotic permeability. The few data collected allow inferring that the electroosmotic permeability of an unsaturated soil might follow a law conceptually similar to that proposed by Archie [Arc42], depending on a power of the water degree of saturation:

$$k_{eo}\left(S_w\right) = k_{eo}^{\ sat}\ k_{eo}^{\ rel} = k_{eo}^{\ sat}\ S_w^{\ \alpha} \tag{33}$$

Data reported in Figure 26 suggest that the electroosmotic permeability decreases with water degree of saturation to a power of about 3, which is intermediate between electric conductivity and hydraulic conductivity.

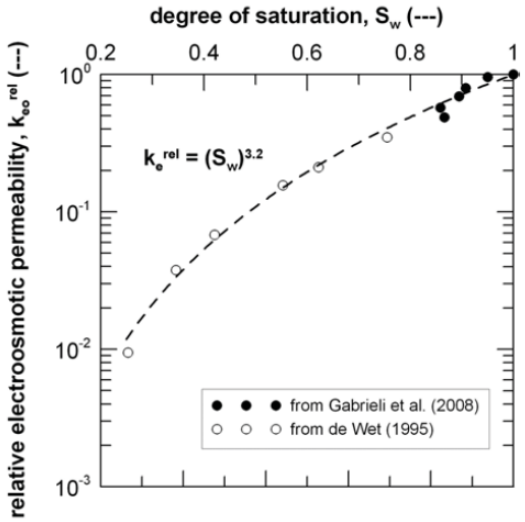

Figure 26: Relative electroosmotic permeability as a function of the water degree of saturation [Tam10].

Ions transport, change in pH, chemical reactions in the aqueous phase and with soil grain constituents may further complicate the simple initial scheme proposed for electroosmotic transport which in reality seldom may be considered a simple and linear coupled water – electric charge transport in porous medium (see, for instance, [Air09]). The merit of Equation (31) is to provide a linearised reference description of this coupled flow around a current equilibrium state.

4 References

[Abu96a] Abu-Hassanein, Z. S., Benson, C. H. and Blotz, L. R. Electrical resistivity of compacted clays. *Journal of Geotechnical Engineering, 122 (5), 397-406*, 1996.

[Abu96b] Abu-Hassanein, Z. S., Benson, C. H., Wang, X., and Blotz, L. R. Determining bentonite content in soil-bentonite mixtures using electrical conductivity. *Geotechnical Testing Journal, 19(1), 51–57*, 1996.

[Air05] Airò Farulla, C. and Ferrari, A. Controlled suction oedometric tests: analysis of some experimental aspects. *Proc. Int. Symposium on Advanced Experimental Unsaturated Soil Mechanics*, Trento, Italy, June 27-29, 2005. Advanced Experimental Unsaturated Soil Mechanics EXPERUS

2005. A. Tarantino, E. Romero and Y.J. Cui (eds.). A.A. Balkema Publishers, Leiden: 43-48, 2005.

[Air09] Airoldi, F., Jommi, C., Musso G., Paglino, E. Influence of calcite on the electrokinetic treatment of a natural clay. *J. Appl. Electrochemistry, 39, 2227-2237*, 2009.

[Alo05] Alonso, E.E., Romero, E., Hoffmann, C. and García-Escudero, E. Expansive bentonite-sand mixtures in cyclic controlled-suction drying and wetting. *Engineering Geology, 81 (3), 213-226*, 2005.

[Ana95] Anandarajah A. and Kuganenthira, N. Some aspects of fabric anisotropy of soil. *Géotechnique, 45(1), 69 –81*, 1995.

[Arc42] Archie, G.E. The electrical resistivity log as an aid to determining some reservoir characteristics. *Trans AIME, 146, 54-63*, 1942.

[Atk10] Atkins P. and De Paula J. *Physical Chemistry*. Oxford University Press, Oxford, 9th ed, 2010.

[Att08] Attia A.M., Fratta D. and Bassiouni Z. Irreducible Water Saturation from Capillary Pressure and Electrical Resistivity Measurements. *Oil & Gas Science and Technology – Rev. IFP, 63(2), 203-217*, 2008. DOI: 10.2516/ogst:2007066.

[Bak09] Baker, R. & Frydman, S. Unsaturated soil mechanics: Critical review of physical foundations. *Engineering Geology, 106(1-2), 26-39*, 2009.

[Bar67] Barden, L. and Sides, G.R. The diffusion of air through the pore water of soils. *Proc. 3rd Asian Reg. Conf. on Soil Mechanics Foundation Engineering*, Israel, 1, 135-138, 1967.

[Ber97] Bernier, F., Volckaert, G., Alonso, E.E. and Villar, M.V. Suction-controlled experiments on Boom clay. *Engineering Geology, 47, 325-338*, 1997.

[Bez09] Bezzar, A. and Ghomari, F. Nondestructive test to track pollutant transport into landfill liners. *Environmental Geology, 57(2), 285–290*, 2009. DOI: 10.1007/s00254-008-1265-5.

[Bla00] Blatz, J. & Graham, J. A system for controlled suction in triaxial tests. *Géotechnique, 50 (4), 465-469*, 2000.

[Bla08] Blatz, J., Cui, Y.J. and Oldecop, L. Vapour equilibrium and osmotic technique for suction control. *Geotechnical and Geological Engineering, 26(6), 661-673,* 2008. DOI: 10.1007/s10706-008-9196-1.

[Ble03] Blewett, J., McCarter, W. J., Chrisp, T. M. and Starrs G. An experimental study on ionic migration through saturated clay. *Engineering Geology, 70, 281-291*, 2003.

[Boc80] Bocking, K.A. and Fredlund, D.G. Limitations of the axis translation technique. *Proc. 4th Int. Conf. on Expansive Soils*, Denver, Colorado: 117-135, 1980.

[Cho04] Cho, G. C.; Lee, J-S. and Santamarina, J.C. Spatial Variability in Soils: High Resolution Assessment with Electrical Needle Probe. *Journal of Geotechnical and Geoenvironmental Engineering, 130 (8), 843-850*, 2004.

[Cui05] Cuisinier, O. and Masrouri, F. Influence de sollicitations hydriques et mécaniques complexes sur le comportement d'un sol gonflant compacté. *Canadian Geotechnical Journal, 42(3), 731–741*, 2005.

[DeG02] De Gennaro, V., Cui, Y.J., Delage, P. and De Laure, E. On the use of high air entry value porous stones for suction control and related problems. *Proc. 3rd Int. Conf. on Unsaturated Soils,* Recife, Brasil, March 10-13, 2002. Unsaturated Soils. J.F.T. Jucá, T.M.P. de Campos and F.A.M. Marinho (eds.). A.A. Balkema Publishers, Lisse, 1: 435-440, 2002.

[Del98] Delage, P., Howat, M.D. and Cui, Y.J. The relationship between suction and swelling properties in a heavily compacted unsaturated clay. *Engineering Geology, 50, 31-48*, 1998.

[Del08a] Delage, P., Romero, E. & Tarantino, A. Recent developments in the techniques of controlling and measuring suction in unsaturated soils. *Unsaturated Soils: Advances in Geo-Engineering, Proc. 1st European Conf. on Unsaturated Soils,* Durham, UK. D.G. Toll, C.E. Augarde, D. Gallipoli and S.J. Wheeler (eds.). CRC Press/Balkema, Leiden: 33-52, 2008.

[Del08b] Delage, P. & Cui, Y.J. An evaluation of the osmotic method of controlling suction. *Geomechanics and Geoengineering: An International Journal, 3(1), 1-11*, 2008. DOI: 10.1080/17486020701868379

[Del05] Delgado A.V., Gonzalez-Caballero F., Hunter R.J., Koopal L.K. and Lyklema J. Measurement and interpretation of electrokinetic phenomena (IUPAC Technical Report). *Pure Appl. Chem., 77 (10), 1753–1805*, 2005. DOI: 10.1351/pac200577101753.

[Due04] Dueck, A. *Hydro-mechanical properties of a water unsaturated sodium bentonite. Laboratory study and theoretical interpretation*. Ph. D. Thesis, Lund University, Sweden, 2004.

[Due07] Dueck, A. Results from suction controlled laboratory tests on unsaturated bentonite – Verification of a model. *Proc. 2nd Int. Conf. Mechanics of*

Unsaturated Soils, Weimar, Germany, March 7-9, 2007. Experimental Unsaturated Soil Mechanics. T. Schanz (ed.). Springer Proceedings in Physics, 112. Springer-Verlag, Berlin: 329-335, 2007.

[Est90] Esteban, F. *Caracterización experimental de la expansividad de una roca evaporítica.* Ph. D. Thesis, Universidad de Cantabria. Spain (in Spanish), 1990.

[Fes07] Festa, C. *Resistivity and seismic methods applied to laboratory soil testing*. PhD Thesis. Politecnico di Torino, 2007.

[Fre77] Fredlund, D.G. and Morgenstern, N.R. Stress state variables for unsaturated soils. *J. Geotech. Engrg. Div., ASCE, 103(5), 447-466*, 1977.

[Fre93] Fredlund, D.G. and Rahardjo, H. *Soil mechanics for unsaturated soils.* John Wiley & Sons, Inc. New York, 1993.

[Fuk99] Fukue, M., Minato, T., Horibe, H. and Taya N. The micro-structures of clay given by resistivity measurements. *Engineering Geology, 54, 43-53*, 1999.

[Fuk01] Fukue M., Minato T., Horibe H. and Taya N. Use of a resistivity cone for detecting contaminated soil layers. *Engineering Geology, 60, 361 – 369*, 2001.

[Gab08a] Gabrieli, L., Jommi, C., Musso G., Romero, E. Influence of electroosmotic treatment on the hydro-mechanical behaviour of clayey silts: preliminary experimental results. *J. Appl. Electrochemistry, 38, 1043-1051*, 2008.

[Gab08b] Gabrieli, L., Jommi, C., Musso G., Romero, E. Electrokinetic treatment of a natural silt in saturated and unsaturated conditions. *Proc. 3rd Int. Symposium GeoProc'2008*. Thermo-Hydromechanical and Chemical Coupling in Geomaterials and Applications. J.-F. Shao and N. Burlion (eds.). ISTE Ltd, London: 203-210, 2008.

[Gar56] Gardner, W.R. Calculation of capillary conductivity from pressure plate outflow data. *Soil Sci. Soc. Am. Proc., 20, 317-320*, 1956.

[Hil56] Hilf, J.W. *An investigation of pore-water pressure in compacted cohesive soils.* PhD Thesis. Technical Memo No.654, United States Bureau of Reclamation, Denver, 1956.

[Hof05] Hoffmann, C., Romero, E. and Alonso, E.E. Combining different controlled-suction techniques to study expansive clays. *Proc. Int. Symposium on Advanced Experimental Unsaturated Soil Mechanics*, Trento, Italy, June 27-29, 2005. Advanced Experimental Unsaturated Soil Mechanics

EXPERUS 2005. A. Tarantino, E. Romero and Y.J. Cui (eds.). A.A. Balkema Publishers, Leiden: 61-67, 2005.

[Hor85] Horvath, A.L. *Handbook of aqueous electrolyte solutions: physical properties, estimation and correlation methods*. Ellis Horword Limited, John Wiley & Sons, New York, 1985.

[Hoy08] Hoyos, L.R., Laloui, L. ad Vassallo, R. Mechanical testing in unsaturated soils. *Geotechnical and Geological Engineering, 26(6), 675-689*, 2008. DOI: 10.1007/s10706-008-9200-9.

[Jot07] Jotisankasa, A., Coop, M. and Ridley, A. The development of a suction control system for a triaxial apparatus. *Geotechnical Testing Journal, 30(1), 1-7*, 2007.

[Kal93] Kalinski, R.J. and Kelly, W. E. Estimating water content of soils from electrical resistivity . *Geotechnical Testing Journal, 16(3), 323-329*, 1993.

[Kle97] Klein, K. and Santamarina, J. C. Methods for Broad-Band Dielectric Permittivity Measurements (Soil-Water Mixtures, 5 Hz to 1.3 GHz), *Geotechnical Testing Journal, 20(2), 168-178*, 1997.

[Kle03] Klein, K. and Santamarina, J. C. Electrical Conductivity in Soils: Underlying Phenomena. *J. Environ. Eng. Geophys., 8(4), 263–273*, 2003.

[Kug96] Kuganenthira, N., Zhao, D. & Anandarajah, A. Measurement of fabric anisotropy in triaxial shearing. *Géotechnique 46(4), 657-670* , 1996.

[Kun62] Kunze, R.J. and Kirkham, D. Simplified accounting for membrane impedance in capillary conductivity determinations. *Soil Sci. Soc. Am. Proc., 26, 421-426*, 1962.

[Law05] Lawrence, C.A., Houston, W.N., Houston, S.L. and Harraz, A.M. Pressure pulse technique for measuring diffused air volume. *Proc. Int. Symposium on Advanced Experimental Unsaturated Soil Mechanics*, Trento, Italy, June 27-29, 2005. Advanced Experimental Unsaturated Soil Mechanics EXPERUS 2005. A. Tarantino, E. Romero and Y.J. Cui (eds.). A.A. Balkema Publishers, Leiden: 9-13, 2005.

[Lid97] Lide, D.R. & Frederikse, H.P.R. CRC *Handbook of chemistry and physics. A ready-reference book of chemical and physical data.* CRC Press, New York, 1997.

[Lee08] Lee, C., Lee, J-S., Lee, W. and Cho T.H. Experiment Setup for Shear Wave and Electrical Resistance Measurements in an Oedometer. *Geotechnical Testing Journal, 31(2), 1 – 7,* 2008.

[Llo85] Lloret, A. & Alonso, E.E. State surfaces for partially saturated soils. *Proc. 11th Int. Conf. on Soil Mechanics and Foundation Engineering,* San Francisco, 2, 557 – 562, 1985.

[Llo03] Lloret, A., Villar, M. V., Sánchez, M., Gens, A., Pintado, X. and Alonso, E. E. Mechanical behaviour of heavily compacted bentonite under high suction changes. *Géotechnique, 53(1), 27–40*, 2003.

[Loc83] Lockhart N.C. Electroosmotic dewatering of clays, III. Influence of clay type, exchangeable cations and electrode materials. *Colloids and Surfaces, 6, 253-269,* 1983.

[Mar08] Marinho, F.A.M., Take, W.A. and Tarantino, A. Measurement of matric suction using tensiometric and axis translation techniques. *Geotechnical and Geological Engineering*, *26(6), 615-631,* 2008. DOI: 10.1007/s10706-008-9201-8.

[Mas08] Masrouri, F., Bicalho, K.V. and Kawai, K. Laboratory hydraulic testing in unsaturated soils. *Geotechnical and Geological Engineering, 26 (6), 691-704*, 2008. DOI: 10.1007/s10706-008-9202-7.

[McC05] McCarter, W J., Blewett, J, Chrisp, T M., Starrs, G. Electrical property measurements using a modified hydraulic oedometer. *Canadian Geotechnical Journal, 42 (2), 655-662(8)*, 2005.

[Mer11] Merchán, V., Romero, E. & Vaunat, J. An adapted ring shear apparatus for testing partly saturated soils in the high suction range. *Geotechnical Testing Journal, 34 (5), 1-12*, 2011.

[Mit05] Mitchell, J.K. and Soga, K. Fundamentals of soil behavior. *John Wiley & Sons*, Hoboken, New Jersey, 2005.

[Mou67] Mousseau, R.J., and R.P. Trump. Measurement of electrical models anisotropy of clay-like materials. *J. Appl. Phys. 38:4375–4379*, 1967.

[Mus00] Musso, G. *Electrokineti phenomena in soils*. Ph.D Thesis, Politecnico di Torino, 2000.

[Mus03] Musso, G., Romero, E., Gens, A. & Castellanos, E. The role of structure in the chemically induced deformations of FEBEX bentonite. *Applied Clay Science, 23, 229-237*, 2003.

[Mus05] Musso, G. and Romero, E. Chemo – mechanical behaviour of high density bentonites. Imbibition and diffusion tests. *Proc. of the Int. Symp. on Large Scale Field Tests in Granite Sitges,* Barcelona, Spain 12-14 Nov. 2003. E.E. Alonso and A. Ledesma (eds.). Balkema, Leiden, The Netherlands, 283-291, 2005.

[Mus09] Musso, G., Casini, F., Colombo, L., Jommi, C. and Springmann, S. Impiego di un ago elettrico per la misura indiretta del contenuto in acqua di campioni non saturi. *Incontro annuale dei ricercatori di Geotecnica, IARG 2009*, Roma, Italy, (in Italian), 2009.

[Old04] Oldecop, L. and Alonso, E.E. Testing rockfill under relative humidity control. *Geotechnical Testing Journal, 27(3), 1-10*, 2004.

[Oli96] Olivella, S., Gens, A., Carrera, J. & Alonso, E.E. Numerical formulation for a simulator (CODE_BRIGHT) for the coupled analysis of saline media. *Engineering computations, 13 (7), 87-112*, 1996.

[Oli06] Oliveira, O.M. and Marinho, F.A.M. Study of equilibration time in the pressure plate. *Proc. 4th Int. Conf. on Unsaturated Soils, Carefree,* Arizona, April 2-6, 2006. Unsaturated Soils. Geotechnical Special Publication No. 147. G.A. Miller, C.E. Zapata, S.L. Houston and D.G. Fredlund (eds.). ASCE, Reston, Virginia, 2, 1864-1874, 2006.

[Pad06] Padilla, J.M., Perera, Y.Y., Houston, W.N., Perez, N. and Fredlund, D.G. Quantification of air diffusion through high air-entry ceramic disks. *Proc. 4th Int. Conf. on Unsaturated Soils, Carefree, Arizona, April 2-6, 2006.* Unsaturated Soils. Geotechnical Special Publication No. 147. G.A. Miller, C.E. Zapata, S.L. Houston and D.G. Fredlund (eds.). ASCE, Reston, Virginia, 2, 1852-1863, 2006.

[Par67] Parkhomenko E.I. *Electrical Properties of Rocks*. Plenum, New York, 1967.

[Pin02] Pintado, X. *Caracterización del comportamiento termo-hidro-mecánico de arcillas expansivas*. Ph. D. Thesis, Universitat Politècnica de Catalunya, Spain (in Spanish), 2002.

[Pin09a] Pintado, X., Lloret, A. & Romero, E. Assessment of the use of the vapour equilibrium technique in controlled-suction tests. *Canadian Geotechnical Journal, 46 (4), 411-423*, 2009. DOI: 10.1139/T08-130

[Pin09b] Pintado, X., Lloret, A. & Romero, E. Reply to the discussion by Leong et al. on 'Assessment of the use of the vapour equilibrium technique in controlled-suction tests'. *Canadian Geotechnical Journal, 46(12), 1485-1486*, 2009. DOI: 10.1139/T09-131

[Ric41] Richards, L.A. A pressure membrane extraction apparatus for soil suction. *Soil Science, 51(5), 377-386*, 1941.

[Rom99] Romero, E. *Characterisation and thermo-hydro-mechanical behaviour of unsaturated boom clay: an experimental study*. PhD Thesis, Universitat Politècnica de Catalunya, Barcelona, Spain, 1999.

[Rom01a] Romero, E. Controlled-suction techniques. *Proc. 4º Simpósio Brasileiro de Solos Nâo Saturados Ñ SAT'2001*. W.Y.Y. Gehling & F. Schnaid (eds.). Porto Alegre, Brasil, 535-542, 2001.

[Rom01b] Romero, E., Gens, A. & Lloret, A. Laboratory testing of unsaturated soils under simultaneous suction and temperature control. *Proc. 15th Int. Conf. on Soil Mechanics and Geotechnical Engineering,* Istanbul, August 27-31, 2001. A.A. Balkema, Rotterdam, 1, 619-622, 2001.

[San01] Santamarina, J.C., Klein, K.A., and Fam, M.A. *Soils and waves*. John Wiley & Sons, Toronto, 2001.

[Sen97] Sen P. N. Resistivity of partially saturated carbonate rocks with microporosity. *Geophysics, 62(2), 415–425*, 1997.

[Spo84] Sposito, G. *The surface chemistry of soils* Oxford University Press, New York, 1984.

[Tam10] Tamagnini, C., Jommi, C., Cattaneo F. A model for coupled electro-hydro-mechanical processes in fine grained soils accounting for gas generation and transport. *Annuals of the Brazilian Academy of Science, 82, 169-193*, 2010.

[Tan05] Tang, A.M., and Cui, Y.J. Controlling suction by the vapour equilibrium technique at different temperatures and its application in determining the water retention properties of MX80 clay. *Canadian Geotechnical Journal, 42, 287-296*, 2005.

[Tan11] Tang, A.M., Cui, Y.J., Qian, L.X., Delage, P. & Ye, W.M. Calibration of the osmotic technique of controlling suction using a miniature tensiometer. *Proc. 5th Asia-Pacific Conf. on Unsaturated Soils,* 29 February – 2 March 2012, Dusit Thani Pattaya, Thailand. Unsaturated Soils: Theory and Practice. A. Jotisankasa, A. Sawangsuriya, S. Soralump and and W. Mairaing (eds.). Kasetsart University, Thailand, 1, 423-427, 2011.

[Tar00] Tarantino, A., Mongiovì, L. and Bosco, G. An experimental investigation on the independent isotropic stress variables for unsaturated soils. *Géotechnique, 50(3), 275-282*, 2000.

[Tar11] Tarantino, A., Gallipoli, D., Augarde, C.E., De Gennaro, V., Gómez, R., Laloui, L., Mancuso, C., El Mountassir, G., Muñoz, J.J., Pereira, J.-M., Peron, H., Pisoni, G., Romero, E., Raveendiraraj, A., Rojas, J.C., Toll, D.G., Tombolato, S. & Wheeler, S. Benchmark of experimental techniques for measuring and controlling suction. *Géotechnique, 61(4), 303–312*, 2011. DOI: 10.1680/geot.2011.61.4.303

[Van08] Vanapalli, S.K., Nicotera, M-V. and Sharma, R.S. Axis translation and negative water column techniques for suction control. *Geotechnical and*

Geological Engineering, *26(6), 645-660*, 2008. DOI: 10.1007/s10706-008-9206-3.

[Vil99] Villar, M.V. Investigation of the behaviour of the bentonite by means of suction-controlled oedometer tests. *Engineering Geology, 54, 67-73*, 1999.

[Wax68] Waxman, M. H., and Smits, L. J. M. Electrical Conductivities in Oil-Bearing Shaly Sands. *Soc. Pet. Eng. J, 8, 107-122*, 1968.

[Wil94] Wilson, G.W., Fredlund, D.G. & Barbour, S.L. Coupled soil - atmosphere modeling for soil evaporation. *Canadian Geotechnical Journal, 31(2), 151-161*, 1994. DOI: 10.1139/t94-021

[Yah99] Yahia-Aissa, M. *Comportement hydromécanique d'une argile gonflante fortement compactée.* Ph. D. Thesis, Ecole Nationale des Ponts et Chaussées, France, 1999.